The effect of HOCl-induced modifications on PTEN structure and function

Verrastro I., Tveen-Jensen K., Spickett C.M., Pitt A.R.

School of Life and Health Science, Aston Triangle, Aston University, Birmingham, B4 7ET, UK

Address for Correspondence: Dr Corinne M. Spickett, School of Life and Health Science, Aston Triangle, Aston University, Birmingham, B4 7ET, UK
Email: c.m.spickett@aston.ac.uk

ABSTRACT

Oxidation by reactive species can cause changes in protein function and affect cell signaling pathways. Phosphatase and tensin homolog (PTEN) is a negative regulator of the PI3K/AKT pathway and is known to be inhibited by oxidation, but its oxidation by the myleoperoxidase-derived oxidant hypochlorous acid (HOCl) has not previously been investigated. PTEN-GST was treated with HOCl:protein ratios from 15:1 to 300:1. Decreases in PTEN phosphatase activity were observed at treatment ratios of 60:1 and higher, which correlated with the loss of the intact protein band and appearance of high molecular weight aggregates in SDS-PAGE. LC-MSMS was used to map oxidative modifications (oxPTMs) in PTEN-GST tryptic peptides and label-free quantitative proteomics used to determine their relative abundance. Twenty different oxPTMs of PTEN were identified, of which 14 were significantly elevated upon HOCl treatment in a dose-dependent manner. Methionine and cysteine residues were the most heavily oxidized; the percentage modification depended on their location in the sequence, reflecting differences in susceptibility. Other modifications included tyrosine chlorination and dichlorination, and hydroxylations of tyrosine, tryptophan, and proline. Much higher levels of oxidation occurred in the protein aggregates compared to the monomeric protein for certain methionine and tyrosine residues located in the C2 and C-terminal domains, suggesting that their oxidation promoted protein destabilization and aggregation; many of the residues modified were classified as buried according to their solvent accessibility. This study provides novel information on the susceptibility of PTEN to the inflammatory oxidant HOCl and its effects on the structure and activity of the protein.

INTRODUCTION

Hypochlorous acid (HOCl) is a reactive molecule produced by neutrophils as an antimicrobial oxidant through the action of the heme-containing enzyme myeloperoxidase (MPO) [1,2]. Its production is triggered by pro-inflammatory stimuli that activate the phagocytes, and it is increased in various pathophysiological states [3-5]. However, because of its significant oxidizing capacity, production of HOCl can also result in oxidative damage to biomolecules of the host tissue, including proteins. HOCl-modified proteins have been detected in diseased tissues, including atherosclerotic plaques [6], bowel tissue obtained from patients affected by inflammatory bowel disease [7], and the glomeruli of patients affected by membranous glomerulonephritis [8]. Interestingly, significant levels of myeloperoxidase expression have been found in brain tissue showing neuropathology, especially in amyloid plaques in Alzheimer's disease [9] and may contribute to the pathology through protein oxidation.

The actions of HOCl on amino acid residues, peptides and proteins have been extensively studied [10-12]. The most susceptible residues are the sulfur containing residues, with methionine being the most reactive [10]. The general susceptibility of methionine to oxidation has resulted in the evolution of protective mechanisms, including methionine sulfoxide reductases [13]. HOCl-mediated oxidation of thiol groups can cause the formation of reversible disulfide bonds potentially leading to protein crosslinking and inactivation [10], other non-specific thiol oxidative products such as cysteine sulfinic and sulfonic acids [4,14,15], and a cyclic sulfonamide product that has been reported to be specific for HOCl oxidation [11]. Evidence of further oxidation of disulfides has also been reported, although the oxidation products are not well characterized [10,16,17]. Reaction of HOCl with the amino groups of proteins can result in the formation of unstable chloramines, which can either be rapidly reduced back to the amine or can break down to give aldehydes [18]. HOCl also reacts with tyrosine residues of proteins to form 3-chlorotyrosine and 3,5-dichlorotyrosine [19]; these reactions are less favored than those with amine groups and thiols, but chlorinated tyrosines are more stable end products of HOCl oxidation than chloramines [18], and have emerged as reliable biomarkers of protein damage by myeloperoxidase [20]. Free chlorinated amino acids have been identified in clinical samples from patients affected by various inflammatory conditions [18,21,22]. It has also been reported that HOCl-induced oxidative damage can cause irreversible formation of protein aggregates *in vivo* [23]; this has attracted interest as a possible factor contributing to the pathophysiology of conditions such as atherosclerosis [24]. The molecular reactions involved in this aggregate formation are not completely understood, but

reports of hypobromous acid protein oxidation induced aggregation [25] and of non-covalent aggregation of proteins on HOCl treatment [26] suggest that amino acid side chain oxidation may play a critical role. HOCl has also been shown to react with the heme-containing enzyme lactoperoxidase, causing heme destruction and aggregation of the protein [27].

Some studies suggest that HOCl is also involved in the modulation of redox-sensitive intracellular signaling pathways, although the major focus of redox signaling has been on hydrogen peroxide. For example, both MPO and HOCl have been implicated in the regulation of cancer-related cellular processes [28], and it has been reported that HOCl is involved in the selective elimination of transformed fibroblast through the induction of apoptosis [29]. Moreover, HOCl has been shown to promote the activation of several cellular pathways via the activation of key proteins such as the tumour suppressor p53 [30], members of the MAP kinase pathway [31] and the iron-regulatory protein 1 [28].

The dual specificity phosphatase PTEN (Phosphatase and tensin homolog) is a negative regulator of the PI3K/Akt pathway and is involved in a number of cellular processes, including metabolism, apoptosis, cell cycle regulation, cell proliferation and survival [32,33]. Much of the research into the oxidative post-translational modifications (oxPTMs) of PTEN has been focused on the redox status of the Cys71 and Cys124 thiols in the active site of the phosphatase, which have been shown to form a reversible disulfide bond that inactivates the protein upon H_2O_2-mediated oxidation [34-36]. We recently showed that such oxidative modification of PTEN also altered its protein interactome, thus potentially affecting its role in signaling pathways [37]. However, no study to date has investigated the effect of HOCl on PTEN activity, or addressed the correlation between oxidation-induced irreversible inactivation and oxidative post-translational modifications (oxPTMs). As HOCl has been shown to induce protein modifications other than reversible thiol oxidation, it is likely that HOCl-specific modifications such as tyrosine chlorination are associated with a permanent alteration of PTEN phosphatase activity and may have adverse effects on its signaling pathways.

The identification of HOCl-specific modifications to proteins is critical to understanding HOCl-mediated regulation of cellular networks [4]. The leading analytical technique for the analysis of oxPTMs is mass spectrometry, as it offers high levels of selectivity and reproducibility for the detection of oxPTMs such as tyrosine chlorination [38]. In this study, LC/MS-based quantitative mapping of HOCl-induced oxidative post-translational modifications (oxPTMs) of PTEN was carried out using a purified GST-tagged PTEN. The purified protein was treated with increasing HOCl concentrations and the modification status of protein residues was compared to the extent of inactivation of phosphatase activity and

aggregation. This functional proteomics approach provided novel information on HOCl-induced oxPTMs of PTEN and their effects.

MATERIALS AND METHODS

Reagents

All reagents were purchased from Fisher Scientific (Loughborough, UK) or Sigma-Aldrich Chemical Co. (Poole, UK) unless otherwise indicated. All solvents were of LC-MS grade and high purity water (>17 MOhms) was used at all times.

HOCl concentration assay

The sodium hypochlorite stock solution was assayed to determine its molar concentration as described previously [39] assuming a molar extinction coefficient of 350 M^{-1} cm^{-1} at $\lambda = 292$ nm under basic conditions [40]. HOCl stock solution was then diluted in 50 mM phosphate buffer pH 7.4 to prepare the solutions for the oxidation experiment.

Expression and purification of PTEN

Glutathione S-transferase (GST)-PTEN cDNA was cloned, overexpressed and purified as described previously [37]. Essentially, *E. coli* DH5α were transformed with the PGEX-4T1-PTEN-GST expression plasmid DNA, grown in the presence of 100 µg/mL ampicillin and protein expression was induced with isopropyl-β-D-1-thiogalactopyranoside. Harvested cells were extracted in 50 mM Tris pH 7.4 containing 2 mg/mL lysozyme, 2 mM EDTA, 2 mM DTT, 1% Triton, and supplemented with EDTA-free protease inhibitor cocktail (Roche Diagnostics GmbH, Mannheim, Germany) by ultrasonication and Potter homogenization before filtering through a 0.45 µm syringe filter (Millipore, Watford, UK). The GST-tagged PTEN was purified at 4ºC by binding to glutathione sepharose 4B beads (GE Healthcare, Little Chalfont, UK) and subsequently eluted with 50 mM Tris pH 7.4, 2 mM DTT, 2.7 mM KCl and increasing NaCl up to 500 mM. Prior to use the purified PTEN-GST was buffer-exchanged into 50 mM phosphate buffer and protein concentration was calculated by absorbance at 280 nm using a Nanodrop c2000 UV-Vis Spectrophotometer (Thermo Fisher Scientific, Hemel Hempstead, UK), using an extinction coefficient of 88,130 M^{-1} cm^{-1}.

Oxidation and activity assay

Purified, buffer-exchanged PTEN-GST was oxidized with 0, 0.5, 1, 2, 5 or 10 mM HOCl (molar ratios of 15:1, 30:1, 60:1, 150:1, and 300:1 respectively) for 1 hour at room temperature. The reaction was stopped by the addition of excess methionine and the phosphatase activity measured by monitoring hydrolysis of the artificial substrate 3-*O*-methylfluorescein phosphate

(OMFP) to 3-*O*-methylfluorescein (OMF), essentially as described by Tierno et al [41]. OMFP was freshly prepared in dimethyl sulfoxide (DMSO) at 20 mM and diluted in assay buffer immediately before use. The final assay contained 15 mM Tris-HCl pH 7.4, 75 mM NaCl, 1 mM EDTA, 1 mM DTT, 160 µM OMFP, 20 µg of protein from the control or HOCl-oxidized samples, and was carried out in a 96-well plate with 250 µL volumes per well. The released 3-*O*-methylfluorescein (OMF) fluorescence was determined with excitation at 485 nm, emission at 525 nm and cutoff at 515 nm continuously over 20 min using a Spectra MAX GEMINI XS Fluorescence plate reader (Molecular Devices Sunnyvale, CA, USA) controlled with the Softmax Pro® software. A standard curve generated by reading serial dilutions of OMF was used to determine protein specific activity. Aliquots of each treatment were also incubated with 100 mM DTT for 15 min prior to assaying the phosphatase activity as described above.

SDS PAGE and Image processing

Fifty µg of HOCl-oxidized PTEN-GST samples were analyzed by SDS-polyacrylamide gel electrophoresis on a 12% gel using standard reducing conditions [42] followed by staining with InstantBlue (Expedeon, Cambridge, UK). Gel densitometry was performed with the Java-based image processing ImageJ [43]. For the full lane gel densitometry, gel images were first imported into Microsoft Powerpoint® and cropped so that white space was left between lanes corresponding to different experimental conditions. The images were saved as .png and opened in ImageJ. All images were converted to 8-bit, background subtracted using a rolling ball radius of 50 pixels and light background, and contrast enhanced by 0.4% of saturated pixels. The stacking gel was included in the crop selection of the full lanes. For the densitometry analysis of the single approximately 70 kDa PTEN band, the gel images were first imported into Microsoft Powerpoint® and cropped so that white space was left between lanes corresponding to different experimental conditions. Next, the lanes were further cropped to include only the protein band at 73 kDa corresponding to PTEN, cropping the image along the edge of the gel band. The images were then saved as .png and opened in ImageJ. All images were converted to 8-bit, and no background subtraction or contrast enhancing was performed.

Protein in-gel digestion

The Coomassie-stained bands corresponding to the intact protein and the protein aggregates were cut out from the gel. The gel pieces were washed twice with 500 µL of 100 mM NH_4HCO_3 and twice with 100 mM NH_4HCO_3/50% acetonitrile. Reduction was performed adding 10 µL of 45 mM DTT (Sigma-Aldrich Chemical Co., Poole, UK) to 150 µL NH_4HCO_3 and incubating at 60ºC for 30 mins. Cysteine alkylation was performed by adding 10 µL of 100 mM iodoacetamide (Sigma-Aldrich Chemical Co., Poole, UK) to 150 and incubating at room

temperature for 30 min in the dark. The gel pieces were washed in 100 mM NH_4HCO_3/50% acetonitrile and incubated in 50 µL of 100% acetonitrile for 10 min. The gel pieces were then dried completely in a centrifugal evaporator and resuspended in 25 µL of 0.1 µg/µL trypsin (Trypsin Gold, Mass Spectrometry Grade, Promega, Southampton, UK) in 50 mM acetic acid or 20 µL of 0.042 µg/µL Lys-C (Endoproteinase LysC Sequencing Grade, Promega, Southampton, UK) resuspended in water. 100 µL 40 mM NH_4HCO_3/10% acetonitrile was added to the trypsin digests, while 40 µL of 25 mM Tris pH 8.5, 1mM EDTA were added to the LysC digests, and the digestions incubated overnight at 37 ℃. The gel pieces were pelleted by centrifugation and the supernatant was collected into a fresh tube. Further peptide extraction from the gel pieces was performed by adding 20 µL 5% formic acid and incubating at 37 ℃ for 20 mins, followed by addition of 40 µL acetonitrile and incubation for 20 mins at 37 ℃. The gel pieces were pelleted by centrifugation, and the supernatant was removed and combined with the first supernatant; this procedure was repeated twice. The peptide extracts were dried completely in a vacuum centrifuge and resuspended in a volume up to 50 µl of 98% H_2O, 2% acetonitrile, 0.1% formic acid (HPLC solvent A) and loaded into screw top glass autosampler vials (Chromacol, Speck and Burke analytical, Clackmannanshire, UK).

Liquid Chromatography-Mass Spectrometry (LC-MS)

Peptides were separated and analyzed using an Ultimate 3000 system (Thermo, Heemel Hempstead, UK) coupled to a 5600 TripleTOF (Sciex, Warrington, UK) controlled by Chromeleon Xpress and Analyst software (TF1.5.1, Sciex, Warrington, UK). Enrichment and desalting of the peptides was achieved using a C18 pre-column (C18 PepMap™, 5 µm, 5 mm × 0.3 mm i.d. Dionex, Bellefonte, PA, US) washing for 4 min with aq. 2% acetonitrile, 0.1% formic acid at 30 µL/min. The peptides were then separated on a C18 nano-HPLC column (C18 PepMap™, 5 µm, 75 µm i.d. × 150 mm, Dionex, Dionex, Camberley, UK) at 300 nL/min using a gradient elution running from 2% to 45% aqueous acetonitrile (0.1% formic acid) over 45 min followed by a washing gradient from 45% to 90% aq. acetonitrile (0.1% formic acid) in 1 min. The system was washed with 90% aq. acetonitrile (0.1% formic acid) for 5 min and then re-equilibrated to the starting solvent. Ionization of the peptides was achieved with spray voltage set at 2.4 kV, a source temperature of 150°C, declustering potential of 50 V and a curtain gas setting of 15. Survey scans were collected in positive mode from 350 to 1250 Da for 200 ms using the high resolution TOF-MS mode. Information-dependent acquisition (IDA) was used to collect MS/MS data using the following criteria: the 10 most intense ions with +2 to +5 charge states and a minimum of intensity of 200 cps were chosen for analysis, using dynamic exclusion for 12s, and standard rolling collision energy setting.

Label-free quantification using Progenesis QI for Proteomics or manual Extracted Ion Chromatogram generation

For the analysis of PTEN modifications, LC-MS runs obtained from the analysis of the HOCl-oxidized PTEN-GST samples were used to generate a total of four separate Progenesis QI experiments, two using the trypsin-digested samples and two using the LysC-digested samples. For each of these, one experiment was generated using the intact PTEN-GST band samples and the other using the protein aggregates sample. Each Progenesis experiment file was generated using a total of 18 LC-MS runs (three independent experiments across six different experimental conditions). The protein identification list was filtered to include only peptides corresponding to PTEN. To analyze PTEN modification, the conflicts between the detected modified peptides were handled as follows: firstly, the MS/MS fragmentation pattern of each conflicting peptide was analyzed by *de novo* sequencing as described below. Where the *de novo* sequencing was not sufficient to resolve the conflicts, the peptide showing the highest Mascot Ion score among the conflicting detected peptides was selected. In the event of conflicting peptides showing equal Mascot Ion score, the peptide showing the highest number of hits was selected. To calculate the relative modification, the summed abundance of the modified peptide was divided by the summed abundance of every other peptide containing the residue in question in the unmodified form (including peptides carrying other modifications). For the analysis of GST modifications, extracted ion chromatograms (XICs) were generated manually for modifications identified using an error tolerant MASCOT search against the complete SwissProt database.

Database Searching

Progenesis-generated .mgf files for both the PTEN peptides from the 70 kDa PTEN-GST band and the protein aggregates LC-MS runs were searched with Mascot. Variable modifications were searched for in groups of 3-5 modifications at a time. Tyrosine chlorination and dichlorination, cysteine dioxidation and trioxidation, methionine oxidation and dioxidation, proline oxidation, tyrosine oxidation, lysine oxidation, tryptophan oxidation, and histidine oxidation were specifically searched for as variable modifications. Carbamidomethyl cysteine was used as a fixed modification. The peptide tolerance used was +/- 0.8 Da, peptide charges of 2+, 3+ and 4+ was used, MS/MS ion search was selected. Other parameters for the searches were as follows: Enzyme: Trypsin; Peptide tolerance: ±0.8 Da; MS/MS tolerance: ±0.8 Da; Peptide charge state: +2, +3 and +4; Max Missed cleavages: 1; #13C: 1; Quantitation: None; Instrument: ESI-QUAD-TOF; Data format: Mascot Generic; Experimental mass values: Monoisotopic; Taxonomy *Homo Sapiens* (Human). To identify GST modifications, an error

tolerant search of the .wiff files generated for the LC-MS runs used for the ProgenesisQI analysis for PTEN was performed against the full SwissProt database with no fixed modifications, and methionine oxidation and cysteine carbamidomethylation as variable modifications.

Solvent Accessible Surface Area Calculations

Residues were classified as buried or exposed according to their solvent accessibility. Class assignment was predicted using GETAREA [44] with a probe diameter of 1.4A (equivalent to water) and the 1d5r.pdb 3D-data file from the PDB database. The higher the ratio the more solvent accessible the residue: ratios <20 are considered buried and >50 exposed. Between these values residues show some solvent accessibility and were classed as intermediate. The N-terminal 13 residues and C-terminal tail (residue 352 onwards) are disordered in the crystal structure so NetsurfP (ver. 1.1) (http://www.cbs.dtu.dk/services/NetSurfP) was used to predict solvent accessibility using the PTEN FASTA sequence obtained from Uniprot. The software predicts relative solvent accessibility (RAS), absolute solvent accessibility (ASA) for each residue, and regions of the protein are divided between exposed and buried by using a cut-off of 25% exposed accessible surface area based on the ASA_{max} of each given amino acid. The Z-score indicates the reliability of the prediction (data points with high Z-scores have lower predicted error compared to data points with low Z-scores) [45].

Statistical analysis

Graph Pad Prism was used for the statistical analysis performed on all data presented in this paper. Activity, densitometry and modifications data within sample types (70 kDa monomer or Aggregates) were analyzed using one-way ANOVA with Dunnett's multiple comparisons test, comparing the values of each treated sample to the mean of the untreated control. Comparisons between 70 kDa monomer or Aggregates at each treatment concentration were made using 2 way ANOVA with Sidak's multiple comparisons test. Correlation between activity and densitometry data was performed using Pearson's correlation analysis. To compare retained activity between two treated samples before and after the reducing wash, two-tailed unpaired Student's t-test was used. $P < 0.05$ was considered significant.

RESULTS

Effect of HOCl oxidation on PTEN phosphatase activity

Following buffer exchange into 50 mM phosphate buffer pH 7.4, PTEN-GST was treated for 1 hour with a 15:1, 30:1, 60:1, 150:1, or 300:1 molar ratio of HOCl to PTEN-GST. HOCl-oxidized samples and untreated control were assayed for phosphatase activity using the OMFP

assay. Increasing molar ratios of HOCl to PTEN-GST were found to correlate with a decrease in PTEN phosphatase activity (**Figure 1A**), with significant loss of activity at ratios of 1:60 and higher. In a separate set of experiments, after oxidation the samples were incubated with 100 mM DTT for 15 min to assess recovery of activity following re-reduction of any inhibitory disulfides formed (**Figure 1B**). This high level of DTT was determined empirically to be necessary to recover full PTEN activity in a 15 minute incubation. Increased activity following the 1 hr DTT incubation was observed even in the control samples, suggesting adventitious oxidation of the active site to the disulfide form during purification of the protein. The specific activities measured for the reduced protein are in good agreement with those reported previously for PTEN [37,46]. The significant variation in control PTEN activity prior to treatment with high levels of DTT is likely to be indicative of the variable oxidation to form the regulatory disulfide occurring during purification, which was only fully reversed following treatment with high DTT, or alternatively some reduction of the disulfide by the 1 mM DTT during sample preparation for the assay. At low levels of oxidant (15:1 and 30:1), no statistically significant loss in recoverable activity, and only a small increase in unrecoverable activity was observed (<10%), which was also not statistically significant. At 60:1 molar ratio, statistically significant activity loss was observed (approximately 75%), of which only approximately 20% could be recovered by DTT treatment. At higher oxidant levels (150:1 and 300:1) activity loss of >90% was observed, which was essentially non-recoverable by DTT treatment.

SDS-PAGE and densitometry analysis of HOCl-oxidized PTEN

HOCl-treated and control samples were analyzed by SDS-PAGE on a 12% gel with samples prepared using reducing sample loading buffer (under standard Laemmli conditions [42]) (**Figure 2**). The intensity of the PTEN-GST band (~70 kDa) decreased with increasing molar ratios of HOCl to PTEN-GST, especially above 60:1 (**Figure 2A**), while the protein staining at molecular weights > 100 kDa in both the resolving and stacking gel increased, most likely corresponding to protein aggregation. Samples treated with 150:1 and 300:1 molar ratios showed little or no PTEN-GST band. ImageJ was used to analyze the Coomassie stained gels quantitatively (**Figure 2B**). The signal intensity corresponding to the PTEN-GST main band decreased following a pattern similar to that of the unrecoverable phosphatase activity (Figure 1B), with a statistically significant reduction in intensity for the sample treated with molar ratio of HOCl to PTEN-GST of 60:1 or greater. However, the total protein signal, generated by

summing the total signal intensity in the lane, was less affected, with the increase in aggregated protein effectively counterbalancing the loss of protein in the main band except in the sample treated with a 300:1 molar ratio of HOCl to PTEN-GST.

Identification and quantification of HOCl-modified PTEN peptides

For each of the HOCl treatments, the bands corresponding to the PTEN-GST main band (~70 kDa) and the areas of gel corresponding to protein aggregation (both in the resolving and stacking gel) were excised, in-gel digested with trypsin and LysC, and analyzed by LC-MS. LC-MS runs were quantitatively analyzed using Progenesis QI for Proteomics or manually generated XICs. For the identification of oxPTMs in PTEN, Mascot database searches were performed in multiple rounds on the aligned LC-MS runs, searching for no more than 5 modifications at a time. Combining the data from the trypsin and Lys-C digestions, the PTEN sequence coverage was 85% for the 70kDa PTEN-GST band, and 82% for the aggregates. The PTEN amino acid sequence with oxidation sites and modifications detected is shown in **Figure 3**. Some residues were missing from the analysis: for example, the catalytic T1-loop (amino acids 160-171) was missing from the analysis of the 70 kDa band and only partially detected in the aggregates (residues 164-172 were not detected). A total of 15 oxidatively modified PTEN amino acids were detected in the peptides generated from the 70 kDa bands and 20 in the protein aggregation area of the gel, with 10 different types of modification detected: methionine sulfoxide and sulfone, cysteine sulfinic and sulfonic acids, 4-hydroxyproline, 5-hydroxytryptophan, 2-oxo-histidine, 3,4-dihydroxyphenylalanine, 3-chlorotyrosine and 3,5-dichlorotyrosine.

Validation of peptide quantification and identification

The Progenesis QI screen view was used to assess the quality of feature matching and differential quantification for relevant peptides. **Figure 4A** shows a representative 3D image corresponding to the 3-chlorotyrosine modified peptide AQEALDFYGEVR (m/z = 716.33, charge = +2), corresponding to PTEN Tyr155 chlorination, in the trypsin-digested 70 kDa band across the six different HOCl treatments. This peptide was also detected in the HOCl-oxidized PTEN-GST aggregate bands and showed a dose-dependent increase in abundance. The modified peptide abundance was highest in the protein sample treated with a 300:1 molar ratio of HOCl to PTEN-GST and lowest in the untreated PTEN-GST sample (maximum fold change = 17.7, ANOVA p-value < 0.0001).

Peptide oxPTM(s) identified by statistical searching were validated by *de novo* sequencing. **Figure 4B** shows *de novo* sequencing of the modified PTEN peptide AQEALDFYGEVR with a 3-chlorotyrosine modification at Tyr155 as an example. This validation demonstrated that the Mascot cutoff score used when filtering the peptide feature identifications in Progenesis QI resulted in no false assignments of oxPTM(s).

Quantitative mapping of HOCl-induced oxPTMs to PTEN

Figure 5 shows the quantitative analysis of all of the oxPTMs of PTEN found in either the 70 kDa protein or the aggregate bands, or both (full data are given in **Supplementary table 1**). Cysteine sulfinic acid was observed only in the 70 kDa monomeric band (Figure 5e), while Tyr240 oxidation, His272 oxidation, Trp274 oxidation and chlorinations of Tyr 377 and 379 (Figure 5 l, o, p. r, s and t respectively) were only observed in aggregates. After statistical analysis, 14 amino acids out of the 20 for which a modification was detected showed a significant increase for at least one HOCl:protein ratio and a fold change ≥ 2.5 in the level of oxidative modification on increasing HOCl treatment; these were Met35, Cys71, Met134, Cys136, Tyr155, Met205, Met239, Tyr240, Met270, His272, Trp274, Tyr315, Tyr377 and Tyr379. The majority of these residues carried only one type of oxPTM; however, Met35 and Cys136 in the 70 kDa band, and Tyr377 in the aggregates showed two different types of oxPTMs.

Methionine residues were, as expected, very susceptible to HOCl-mediated oxidation to both sulfoxide and sulfone, although in many cases significant methionine oxidation to the sulfoxide was also found in the untreated control. In the 70 kDa band Met134, Met239, and Met270 reached approximately a 70% modification with the highest HOCl concentrations compared to 10-20% in the untreated control. Met205 was up to 38% oxidized to sulfoxide in the aggregated protein but was not detected in the intact PTEN-GST band. Met35 showed increased oxidation to the sulfone, with approximately 10% sulfone generated upon >150:1 treatment in both intact band and aggregates. HOCl treatment was also found to give extensive cysteine oxidation. Cys71, the PTEN active site regulatory cysteine, was significantly more oxidized to the sulfonic acid in treatments >150:1 in the 70 kDa band, and at treatments >30:1 in the aggregates fraction. Treatments >150:1 caused a significant increase in Cys136 sulfonic acid (to 80% oxidized to in the 70 kDa band and >90% in the aggregates for all samples) and a low level of oxidation to the sulfinic acid was also detected at in the 70 kDa band. At >60:1 treatment Cys250 was significantly more oxidized to sulfonic acid in all bands, with a peak modification level of approximately 50%. Interestingly, very low oxidation levels of the active

site cysteine (less than 2%) were detected for all oxidant concentrations (**Supplementary figure 1a**). However, the level of the unmodified peptide containing this residue normalized against another peptide that did not contain easily oxidized residues (m/z 462.8, residues 190-197, PVALLFHK) did drop to some extent with increasing oxidant concentration, especially in the 70 kDa band (**Supplementary figure 1b**), although a concomitant increase in this peptide carrying other modifications could not be detected. This is likely to be due to the low signal for this large peptide, coupled to the heterogeneity of oxidation that could occur at other residues within it.

HOCl treatment also resulted in the chlorination of several tyrosine residues in both the 70 kDa band and aggregate band. Tyr155 showed a maximum level of 10% chlorination in the 70 kDa band and 15% in the aggregates upon 300:1 treatment, and Tyr315 gave a maximum modification level of approximately 10% in the 70 kDa band and 5% in the aggregates at higher level treatments. Tyr377 was significantly more modified in the aggregates but not in the intact PTEN-GST band, with a maximum of 15% chlorination and 10% dichlorination at 300:1 treatment. In the aggregate fraction, but not in the intact band, significantly higher levels of hydroxylation of aromatic amino acids were detected, including tyrosine, histidine and tryptophan. Hydroxylation of tyrosine was significantly higher on HOCl treatment, although the overall levels were low (maximum approximately 6%). His272 and Trp274 showed a significant increase in hydroxylation at >150:1 treatment with maximal modification levels >20% in the samples treated more aggressively. Oxidative modification to the GST tag were also analyzed for the 70 kDa band and aggregates, and showed a similar behavior to PTEN, in that the extent of modification was very residue specific; example data are shown in **Supplementary figure 2**. Chlorination of Tyr33 and oxidation of Trp41, both of which are located in the globular core of the protein, are found mainly in the aggregates, with up to 15% chlorination of Tyr33 detected, whereas oxidation of Met94 to sulfoxide and sulfone occurs approximately equally in both the 70 kDa and aggregate bands.

DISCUSSION

It is well-established that PTEN can be redox-regulated by formation of a disulphide between the catalytic Cys124 and the regulatory Cys71, and is therefore sensitive to oxidation by H_2O_2 [34,35,37], but the effect of the myeloperoxidase-derived oxidant HOCl on PTEN activity and amino acid residue modification has not previously been investigated. This study describes the effect of HOCl-induced oxidative modification of a GST-tagged PTEN. The oxidations were carried out at physiological pH (7.4) in order that amino acid side chains were

13

in the most relevant ionization states. The pKa of HOCl is 7.59, so at this pH the HOCl:OCl⁻ ratio is approximately 1:1 [40]; in the absence of metal ions decomposition of HOCl to chlorate is reported to be slow [47], and thus the major route of HOCl consumption is likely to be reaction with protein amino acid side chains [10]. A range of HOCl to PTEN-GST molar ratios from 15:1 to 300:1 were found to cause inactivation of the protein, oxidations to a variety of amino acid residues, as well as chlorinations of tyrosine, which are recognized as specific markers of myeloperoxidase- and HOCl-induced protein damage [48-50]. DTT-reversible loss of activity was detected even at low oxidant concentrations, but these lower levels of treatment had little effect on DTT-recoverable protein activity, whereas at higher treatment ratios significant irreversible loss of activity was observed, in parallel with the formation of protein aggregates. The concentrations of HOCl that we found were required to observe these effects in vitro are significantly higher than the levels reported to be present in vivo of up to 400 μM [51]. We used the higher levels to induce the modifications that might occur in vivo under conditions of chronic inflammation where, while HOCl levels may be lower than we used in vitro, irreversible modifications could be introduced and accumulate over the extended exposure time.

The activity of untreated PTEN could be increased by incubation with high levels of DTT, suggesting that the protein was already partially inactivated by disulphide bond formation during purification, and that the 1 mM DTT present in the phosphatase assay was insufficient to fully reverse this. In our hands, treatment with 100mM DTT for 15 minutes was necessary to recover maximal activity. This resistance to re-reduction may partially explain the need for the thioredoxin-mediated reduction of PTEN in vivo [52]. Exposing PTEN to HOCl caused a dose-dependent decrease in PTEN activity that was reversible at low and partially reversible at an intermediate HOCl:PTEN ratio by high DTT concentrations (compatible with disulfide formation) but was not reversible at higher treatment concentrations. Despite good protein sequence coverage (80-85%), data on the peptide containing the catalytic Cys124 was challenging to obtain; the tryptic peptide is 41 residues long and contains many oxidizable residues (1 Tyr, 1 Phe, 3 His, 1 Lys and 1 Trp as well as cysteines 105 and 124). We were able to detect and identify the unmodified peptide and to measure the % modification of the active site cysteine 124 to the sulfonic acid. Unlike the other cysteine residue oxidations observed (e.g Cys136), the % modification of Cys124 was low (< 2%) and did not appear to increase significantly with increasing oxidant concentration. This low level of active site Cys124 modification may indicate that this is protected from over oxidation by the rapid formation of a disulfide with the resolving Cys71.

It is also possible that modification of other residues could have contributed to the loss of activity. Of the 20 PTEN modified residues mapped and quantified, 14 were significantly more modified following HOCl treatment; these included methionine sulfoxide and sulfone, cysteine sulfinic and sulfonic acid, tyrosine hydroxylation, chlorination and dichlorination, histidine hydroxylation and tryptophan hydroxylation. These oxidation sites were mapped on the PTEN 3D crystal structure obtained from the Protein Data Bank (PDB) ID 1D5R using the UCSF Chimera Molecular Modeling software to indicate the solvent exposure and their distribution throughout the protein structure (**Figure 6A**). The relationship between maximum extent of modification and fold-increase in modification was determined and plotted in **Figure 6B**. It is interesting that residues divide roughly into 2 categories: those that could be highly modified but did not show large fold changes compared to the control, and those with very high fold increases in oxidation, which tended to occur at low levels in the controls. This is in agreement with the concept that residues can differ substantially in their susceptibility to oxidation depending on their nature and location in the protein [12,53,54]. Most methionine residues were found to be extensively modified, in agreement with previous findings on their susceptibility to HOCl [12,55], but their modification profile varied significantly in different locations. In view of the fact that there was no significant decrease in phosphatase activity until treatment ratios greater than 30:1, it can be concluded that modifications that increase at lower treatment ratios do not affect activity significantly. No individual residue monitored had an oxidation profile in the 70kD band that closely matched the activity profile, where the major loss occurred between 30: and 60:1 HOCl ratios.

Loss of enzymatic activity could also result indirectly from general structural disruption and (partial) unfolding of the protein, which is likely to lead to aggregation owing to exposure of core hydrophobic residues [56]. There was a strong correlation between the loss of the 70 kDa band for the intact protein signal and the decrease in phosphatase activity (r = 0.936; p-value = 0.006). In parallel, the formation of high molecular mass aggregates on polyacrylamide gels were observed following treatment with high HOCl ratios; these aggregates were resistant to solubilization by detergent and thiol-reducing reagents during the sample preparation. This could be due to formation of alternative covalent cross-links, such as dityrosine formation, or non-covalent aggregation that was resistant to solubilisation. For many residues, the profile of oxidation differed between the native protein and the aggregates; Met134 sulfone and Cys136 sulfinic acid were only observed in the 70 kD band, whereas modifications of Met198, Met 199, Met205, Tyr225, Tyr240, His 272, Trp274, Tyr377 and Tyr379 were only found in PTEN aggregates. Cysteine sulfonic acids on Cys136, Cys250 and Cys71 also occurred at higher

15

proportions in the PTEN aggregates. In contrast, Met35 and Met239 sulfoxides occurred at very similar levels in both native and aggregated PTEN.

The differences in levels of oxidation between native PTEN and PTEN aggregates raise interesting questions about how oxidation of specific residues affects the stability of the protein. It is not possible to determine cause and effect in this study, but the observation of substantial levels of certain modifications only in aggregates suggests that their formation may lead to destabilization of the native structure, and rapid conversion to an aggregated form. Most of the residues observed preferentially in the aggregates were located either in the C2 domain (Met 198-Trp274) or in the C-terminal tail (Tyr377 and Tyr379). As a stabilization role has been proposed for both the C2 domain of PTEN [57] and the C-terminal tail [58,59], it is possible that modification of these residues decreases protein stability and contributes to the increased PTEN aggregation observed at higher HOCl ratios. The presence of Met oxidation in oxidation-inducible protein aggregates has been reported previously, although is unclear whether the modification occurs before or after formation of the aggregates [60,61]. It is important to note that although a high % oxidation of certain residues (e.g. Met35 and Met270) was observed in aggregates at low HOCl treatment ratios, the amount of aggregates in these samples was very low, therefore the total amount of oxidation was also low. Finally, it is important to consider that as the PTEN was a fusion protein with GST and oxidative modifications to the GST were also observed in the aggregate bands, these could contribute to protein aggregation.

Recent studies have reported that oxidation of surface-exposed redox-sensitive amino acids is a primary event that promotes protein misfolding and aggregation [62,63]. Consequently, the solvent accessibility of the modified residues was predicted with NetsurfP and is shown in Table 1 for all residues in Figure 5. Solvent accessibility data obtained for all 403 PTEN amino acids are reported in Supplementary Table 2. It was noted that the majority of the oxPTMs detected after HOCl treatment were residues that under normal folding conditions are inaccessible to the surface solvent and hence should be protected from oxidation [64]. However, published data support the concept that HOCl can oxidize buried hydrophobic residues such as methionine [23,65], and Fu et al. suggest that oxidation of methionines converts them from a hydrophobic to a hydrophilic form, and would be expected to lead to large conformational changes [65]. The exceptions were Met205, Tyr240 and Tyr377, which mapped to regions of the proteins predicted to be solvent-exposed and were detected exclusively in the aggregates fraction. The profile of oxidation of Tyr240 and chlorination of Tyr377 matched better with aggregate formation than Met205, which was oxidized

substantially at lower treatment concentrations. One explanation could be that HOCl-induced aggregation may occur through the initial oxidation of a small number of exposed surface residues, resulting in some disruption of the structure leading to exposure of more buried residues, which can then also become oxidized leading to further, more extensive unfolding and aggregation.

The oxidative modifications observed in PTEN occur in a number of residues that have been reported to have functional effects and may therefore have physiological importance. Tyr155, which was chlorinated, has been shown by mutagenesis to be required for PTEN catalytic activity [66], as well as for the regulation of PTEN interaction with the E3 ubiquitin ligase WWP2, which mediates degradation of PTEN through an ubiquitination-dependent pathway [67]. It has been reported that mutation of either Tyr240 or Tyr315 causes a decrease in both phosphatase activity and PTEN tumour suppressing function [68]. Trp274 has been identified as a cancer-related mutation site in PTEN [69] and Met 134 has previously been identified as a PTP mutational hotspot [70], so oxidative damage to these residues may be important in cancer progression, which is known to be linked to inflammation and oxidative imbalance [71].

In summary, we report for the first time the effect of HOCl-mediated damage on the activity and structure of the phosphatase PTEN. The LC-MS-based quantitative mapping identified oxPTMs at residues important for PTEN activity and protein-protein interactions, and suggested residues that contribute to oxidative unfolding and aggregation. However, a limitation of the study was that some residues located in the T1-loop, CBR3-loop, and the cα2 helix were not observed, and also the method used in this study does not enable the identification of disulfide bonds, as they are reduced and alkylated during sample preparation. Data interpretation is also complicated by the fact that the oxidation process leads to heterogeneous products: while the overall sample has all the modifications observed, any single protein molecule may have only a sub-set of them. Bottom up proteomics provides information on a population of peptides from multiple protein molecules without to the possibility of determining which individual molecule they came from. This is a challenge that still needs to be overcome to understand fully the effect of oxPTMs on PTEN phosphatase activity and folding status. Nevertheless, the proteomics approach described holds a great potential for measuring the effects of oxidation on proteins. To understand fully the biological relevance of these effect will require the application of this approach to assess PTEN oxidation status in stressed or stimulated cells.

ABBREVIATIONS

ASA, Absolute solvent accessibility; DTT, Dithiothreitol; FC, Fold change; GSH, glutathione (reduced form); GST, Glutathione-S-transferase; LC, liquid chromatography; MS, Mass spectrometry; OMFP, 3-*O*-methylfluorescein phosphate; oxPTMs, oxidative post-translational modifications; PTEN, Phosphatase and tensin homolog; RAS, relative solvent accessibility.

ACKNOWLEDGEMENTS

REFERENCES

[1]   Harrison JE, Schultz J. Studies on the chlorinating activity of myeloperoxidase. J Biol Chem 1976;251(5):1371-4.

[2]   Nauseef WM. Myeloperoxidase in human neutrophil host defence. Cell Microbiol 2014;16(8):1146-55.

[3]   Sugiyama S, Okada Y, Sukhova GK, Virmani R, Heinecke JW, Libby P. Macrophage myeloperoxidase regulation by granulocyte macrophage colony-stimulating factor in human atherosclerosis and implications in acute coronary syndromes. Am J Pathol 2001;158(3):879-91.

[4]   Pitt AR, Spickett CM. Mass spectrometric analysis of HOCl- and free-radical-induced damage to lipids and proteins. Biochem Soc Trans 2008;36(Pt 5):1077-82.

[5]   Whiteman M, Hooper DC, Scott GS, Koprowski H, Halliwell B. Inhibition of hypochlorous acid-induced cellular toxicity by nitrite. Proc Natl Acad Sci U S A 2002;99(19):12061-6.

[6]   Hazen SL, Heinecke JW. 3-Chlorotyrosine, a specific marker of myeloperoxidase-catalyzed oxidation, is markedly elevated in low density lipoprotein isolated from human atherosclerotic intima. J Clin Invest 1997;99(9):2075-81.

[7]   McKenzie SJ, Baker MS, Buffinton GD, Doe WF. Evidence of oxidant-induced injury to epithelial cells during inflammatory bowel disease. J Clin Invest 1996;98(1):136-41.

[8]   Grone HJ, Grone EF, Malle E. Immunohistochemical detection of hypochlorite-modified proteins in glomeruli of human membranous glomerulonephritis. Lab Invest 2002;82(1):5-14.

[9]   Green PS, Mendez AJ, Jacob JS, Crowley JR, Growdon W, Hyman BT, Heinecke JW. Neuronal expression of myeloperoxidase is increased in Alzheimer's disease. J Neurochem 2004;90(3):724-33.

[10]   Pattison DI, Davies MJ. Absolute rate constants for the reaction of hypochlorous acid with protein side chains and peptide bonds. Chem Res Toxicol 2001;14(10):1453-64.

[11]   Davies MJ. The oxidative environment and protein damage. Biochim Biophys Acta 2005;1703(2):93-109.

[12]   Davies MJ. Protein oxidation and peroxidation. Biochem J 2016;473(7):805-25.

[13] Cabreiro F, Picot CR, Friguet B, Petropoulos I. Methionine sulfoxide reductases: relevance to aging and protection against oxidative stress. Ann N Y Acad Sci 2006;1067:37-44.

[14] Bruschi M, Candiano G, Santucci L, Ghiggeri GM. Oxidized albumin. The long way of a protein of uncertain function. Biochim Biophys Acta 2013;1830(12):5473-9.

[15] Stacey MM, Vissers MC, Winterbourn CC. Oxidation of 2-cys peroxiredoxins in human endothelial cells by hydrogen peroxide, hypochlorous acid, and chloramines. Antioxid Redox Signal 2012;17(3):411-21.

[16] Nagy P, Ashby MT. Reactive sulfur species: kinetics and mechanism of the oxidation of cystine by hypochlorous acid to give N,N'-dichlorocystine. Chem Res Toxicol 2005;18(6):919-23.

[17] Storkey C, Davies MJ, Pattison DI. Reevaluation of the rate constants for the reaction of hypochlorous acid (HOCl) with cysteine, methionine, and peptide derivatives using a new competition kinetic approach. Free Radic Biol Med 2014;73:60-6.

[18] Pryor WA. Bio-assays for oxidative stress status (BOSS). New York: Elsevier; 2001. ix, 286 p. p.

[19] Kang JI, Jr., Neidigh JW. Hypochlorous acid damages histone proteins forming 3-chlorotyrosine and 3,5-dichlorotyrosine. Chem Res Toxicol 2008;21(5):1028-38.

[20] Kettle AJ, Albrett AM, Chapman AL, Dickerhof N, Forbes LV, Khalilova I, Turner R. Measuring chlorine bleach in biology and medicine. Biochim Biophys Acta 2014;1840(2):781-93.

[21] Sochaski MA, Jarabek AM, Murphy J, Andersen ME. 3-chlorotyrosine and 3,5-dichlorotyrosine as biomarkers of respiratory tract exposure to chlorine gas. J Anal Toxicol 2008;32(1):99-105.

[22] Westman E, Lundberg K, Erlandsson Harris H. Arthritogenicity of collagen type II is increased by chlorination. Clin Exp Immunol 2006;145(2):339-45.

[23] Winter J, Ilbert M, Graf PC, Ozcelik D, Jakob U. Bleach activates a redox-regulated chaperone by oxidative protein unfolding. Cell 2008;135(4):691-701.

[24] Podrez EA, Abu-Soud HM, Hazen SL. Myeloperoxidase-generated oxidants and atherosclerosis. Free Radic Biol Med 2000;28(12):1717-25.

[25] Hawkins CL, Davies MJ. The role of aromatic amino acid oxidation, protein unfolding, and aggregation in the hypobromous acid-induced inactivation of trypsin inhibitor and lysozyme. Chem Res Toxicol 2005;18(11):1669-77.

[26] Chapman AL, Winterbourn CC, Brennan SO, Jordan TW, Kettle AJ. Characterization of non-covalent oligomers of proteins treated with hypochlorous acid. Biochem J 2003;375(Pt 1):33-40.

[27] Souza CE, Maitra D, Saed GM, Diamond MP, Moura AA, Pennathur S, Abu-Soud HM. Hypochlorous acid-induced heme degradation from lactoperoxidase as a novel mechanism of free iron release and tissue injury in inflammatory diseases. PLoS One 2011;6(11):e27641.

[28] Mutze S, Hebling U, Stremmel W, Wang J, Arnhold J, Pantopoulos K, Mueller S. Myeloperoxidase-derived hypochlorous acid antagonizes the oxidative stress-mediated activation of iron regulatory protein 1 (vol 278, pg 40542, 2003). J Biol Chem 2003;278(49):49662-49662.

[29] Herdener M, Heigold S, Saran M, Bauer G. Target cell-derived superoxide anions cause efficiency and selectivity of intercellular induction of apoptosis. Free Radic Biol Med 2000;29(12):1260-71.

[30] Vile GF, Rothwell LA, Kettle AJ. Hypochlorous acid activates the tumor suppressor protein p53 in cultured human skin fibroblasts. Arch Biochem Biophys 1998;359(1):51-6.

[31] Midwinter RG, Vissers MC, Winterbourn CC. Hypochlorous acid stimulation of the mitogen-activated protein kinase pathway enhances cell survival. Arch Biochem Biophys 2001;394(1):13-20.

[32] Georgescu MM. PTEN tumor suppressor network in PI3K-Akt pathway control. Genes Cancer 2010;1(12):1170-7.

[33] Yin Y, Shen WH. PTEN: a new guardian of the genome. Oncogene 2008;27(41):5443-53.

[34] Kwon J, Lee SR, Yang KS, Ahn Y, Kim YJ, Stadtman ER, Rhee SG. Reversible oxidation and inactivation of the tumor suppressor PTEN in cells stimulated with peptide growth factors. Proc Natl Acad Sci U S A 2004;101(47):16419-24.

[35] Lee SR, Yang KS, Kwon J, Lee C, Jeong W, Rhee SG. Reversible inactivation of the tumor suppressor PTEN by H2O2. J Biol Chem 2002;277(23):20336-42.

[36] Leslie NR, Bennett D, Lindsay YE, Stewart H, Gray A, Downes CP. Redox regulation of PI 3-kinase signalling via inactivation of PTEN. EMBO J 2003;22(20):5501-10.

[37] Verrastro I, Tveen-Jensen K, Woscholski R, Spickett CM, Pitt AR. Reversible oxidation of phosphatase and tensin homolog (PTEN) alters its interactions with signaling and regulatory proteins. Free Radic Biol Med 2016;90:24-34.

[38] Verrastro I, Pasha S, Jensen KT, Pitt AR, Spickett CM. Mass spectrometry-based methods for identifying oxidized proteins in disease: advances and challenges. Biomolecules 2015;5(2):378-411.

[39] Jerlich A, Pitt AR, Schaur RJ, Spickett CM. Pathways of phospholipid oxidation by HOCl in human LDL detected by LC-MS. Free Radic Biol Med 2000;28(5):673-82.

[40] Morris JC. The Acid Ionization Constant of HOCl from 5 to 35°. The Journal of Physical Chemistry 1966;70(12):3798-3805.

[41] Tierno MB, Johnston PA, Foster C, Skoko JJ, Shinde SN, Shun TY, Lazo JS. Development and optimization of high-throughput in vitro protein phosphatase screening assays. Nat Protoc 2007;2(5):1134-44.

[42] Laemmli UK. Cleavage of structural proteins during the assembly of the head of bacteriophage T4. Nature 1970;227(5259):680-5.

[43] Schneider CA, Rasband WS, Eliceiri KW. NIH Image to ImageJ: 25 years of image analysis. Nature Methods 2012;9(7):671-675.

[44] Fraczkiewicz R, Braun W. Exact and efficient analytical calculation of the accessible surface areas and their gradients for macromolecules. Journal of Computational Chemistry 1998;19(3):319-333.

[45] Petersen B, Petersen TN, Andersen P, Nielsen M, Lundegaard C. A generic method for assignment of reliability scores applied to solvent accessibility predictions. BMC Struct Biol 2009;9:51.

[46] Mak LH, Vilar R, Woscholski R. Characterisation of the PTEN inhibitor VO-OHpic. J Chem Biol 2010;3(4):157-63.

[47] Adam LC, Fabian I, Suzuki K, Gordon G. Hypochlorous acid decomposition in the pH 5-8 region. Inorganic Chemistry 1992;31(17):3534-3541.

[48] Steinbeck MJ, Nesti LJ, Sharkey PF, Parvizi J. Myeloperoxidase and chlorinated-peptides in osteoarthritis: Potential biomarkers of the disease. J Bone Miner Res 2006;21:S144-S144.

[49] Shao B, Pennathur S, Heinecke JW. Myeloperoxidase targets apolipoprotein A-I, the major high density lipoprotein protein, for site-specific oxidation in human atherosclerotic lesions. J Biol Chem 2012;287(9):6375-86.

[50] Buss IH, Senthilmohan R, Darlow BA, Mogridge N, Kettle AJ, Winterbourn CC. 3-Chlorotyrosine as a marker of protein damage by myeloperoxidase in tracheal

aspirates from preterm infants: association with adverse respiratory outcome. Pediatr Res 2003;53(3):455-62.

[51] King CC, Jefferson MM, Thomas EL. Secretion and inactivation of myeloperoxidase by isolated neutrophils. Journal of Leukocyte Biology 1997;61(3):293-302.

[52] Schwertassek U, Haque A, Krishnan N, Greiner R, Weingarten L, Dick TP, Tonks NK. Reactivation of oxidized PTP1B and PTEN by thioredoxin 1. FEBS J 2014;281(16):3545-58.

[53] Szuchman-Sapir AJ, Pattison DI, Ellis NA, Hawkins CL, Davies MJ, Witting PK. Hypochlorous acid oxidizes methionine and tryptophan residues in myoglobin. Free Radic Biol Med 2008;45(6):789-98.

[54] Aledo JC, Canton FR, Veredas FJ. Sulphur Atoms from Methionines Interacting with Aromatic Residues Are Less Prone to Oxidation. Sci Rep 2015;5:16955.

[55] Malle E, Marsche G, Arnhold J, Davies MJ. Modification of low-density lipoprotein by myeloperoxidase-derived oxidants and reagent hypochlorous acid. Biochim Biophys Acta 2006;1761(4):392-415.

[56] Jung T, Hohn A, Grune T. The proteasome and the degradation of oxidized proteins: Part II - protein oxidation and proteasomal degradation. Redox Biol 2014;2:99-104.

[57] Georgescu MM, Kirsch KH, Kaloudis P, Yang H, Pavletich NP, Hanafusa H. Stabilization and productive positioning roles of the C2 domain of PTEN tumor suppressor. Cancer Res 2000;60(24):7033-8.

[58] Valiente M, Andres-Pons A, Gomar B, Torres J, Gil A, Tapparel C, Antonarakis SE, Pulido R. Binding of PTEN to specific PDZ domains contributes to PTEN protein stability and phosphorylation by microtubule-associated serine/threonine kinases. J Biol Chem 2005;280(32):28936-43.

[59] Vazquez F, Ramaswamy S, Nakamura N, Sellers WR. Phosphorylation of the PTEN tail regulates protein stability and function. Mol Cell Biol 2000;20(14):5010-8.

[60] Torosantucci R, Mozziconacci O, Sharov V, Schoneich C, Jiskoot W. Chemical modifications in aggregates of recombinant human insulin induced by metal-catalyzed oxidation: covalent cross-linking via michael addition to tyrosine oxidation products. Pharm Res 2012;29(8):2276-93.

[61] Luo Q, Joubert MK, Stevenson R, Ketchem RR, Narhi LO, Wypych J. Chemical modifications in therapeutic protein aggregates generated under different stress conditions. J Biol Chem 2011;286(28):25134-44.

[62] Samson AL, Knaupp AS, Kass I, Kleifeld O, Marijanovic EM, Hughes VA, Lupton CJ, Buckle AM, Bottomley SP, Medcalf RL. Oxidation of an exposed methionine instigates the aggregation of glyceraldehyde-3-phosphate dehydrogenase. J Biol Chem 2014;289(39):26922-36.

[63] Tornvall U. Pinpointing oxidative modifications in proteins-recent advances in analytical methods. Anal Methods 2010;2(11):1638-1650.

[64] Levine RL, Moskovitz J, Stadtman ER. Oxidation of methionine in proteins: Roles in antioxidant defense and cellular regulation. Iubmb Life 2000;50(4-5):301-307.

[65] Fu X, Chen J, Gallagher R, Zheng Y, Chung DW, Lopez JA. Shear stress-induced unfolding of VWF accelerates oxidation of key methionine residues in the A1A2A3 region. Blood 2011;118(19):5283-91.

[66] Andres-Pons A, Rodriguez-Escudero I, Gil A, Blanco A, Vega A, Molina M, Pulido R, Cid VJ. In vivo functional analysis of the counterbalance of hyperactive phosphatidylinositol 3-kinase p110 catalytic oncoproteins by the tumor suppressor PTEN. Cancer Res 2007;67(20):9731-9.

[67] Maddika S, Kavela S, Rani N, Palicharla VR, Pokorny JL, Sarkaria JN, Chen J. WWP2 is an E3 ubiquitin ligase for PTEN. Nat Cell Biol 2011;13(6):728-33.

[68]   Koul D, Jasser SA, Lu YL, Davies MA, Shen RJ, Shi YX, Mills GB, Yung WKA. Motif analysis of the tumor suppressor gene MMAC/PTEN identifies tyrosines critical for tumor suppression and lipid phosphatase activity. Oncogene 2002;21(15):2357-2364.

[69]   Naguib A, Bencze G, Cho H, Zheng W, Tocilj A, Elkayam E, Faehnle CR, Jaber N, Pratt CP, Chen MH and others. PTEN functions by recruitment to cytoplasmic vesicles. Molecular Cell 2015;58(2):255-268.

[70]   Myers MP, Stolarov JP, Eng C, Li J, Wang SI, Wigler MH, Parsons R, Tonks NK. P-TEN, the tumor suppressor from human chromosome 10q23, is a dual-specificity phosphatase. Proc Natl Acad Sci U S A 1997;94(17):9052-9057.

[71]   Glasauer A, Chandel NS. Targeting antioxidants for cancer therapy. Biochem Pharmacol 2014;92(1):90-101.

FIGURE LEGENDS

Figure 1. HOCl irreversibly inactivates PTEN at higher treatment ratios. (A) The OMFP assay was used to monitor the effect of increasing HOCl to PTEN-GST molar ratios on PTEN specific activity. The results are presented as mean ± SD (n = 4). Statistical significance for different to the untreated control was assessed by one-way ANOVA followed by Dunnett's correction for multiple comparisons. PTEN specific activity is expressed in nmol OMF/min/mg protein. (B) The effect of DTT reduction on the phosphatase activity of HOCl-oxidized PTEN was evaluated by comparing the specific activity retained by the HOCl-oxidized PTEN before and after recovery with 100 mM DTT. The results are presented as mean ± SD (n = 3). Statistical significance was assessed by two-tailed unpaired Student's t-test for each HOCl:protein ratio. Untr = untreated; * = $p < 0.05$; ** = $p < 0.01$; *** = $p < 0.001$; **** = $p < 0.0001$; ns = not significant).

Figure 2. SDS-PAGE/densitometry analysis versus phosphatase activity of HOCl-oxidized PTEN-GST. (A) Representative (of n=3) Coomassie-stained gel of HOCl-oxidized PTEN-GST. 50 µg of protein was loaded per well. Untr = 0 mM HOCl; MW = molecular weight markers. (B) The percentage signal intensity of the Coomassie-stained intact PTEN-GST band and the full gel lane analyzed by densitometry were plotted versus the percentage phosphatase activity as a % of control. Statistical analysis was performed with one-way ANOVA followed by Dunnett's multiple comparisons test before baseline correction. Densitometry data are presented as mean ± SD for N= 3 and activity data are presented as mean ± SD for N = 4 (* = $p < 0.05$; *** = $p < .001$; **** = $p < 0.0001$). (C) Correlation between PTEN phosphatase activity and the protein signal on the gel corresponding to the PTEN-GST band or the full lane. The correlation coefficient r and the p-value were calculated using Pearson's correlation analysis.

Figure 3. PTEN sequence coverage and oxidation sites identified from LC-MS/MS data. For both intact band and aggregate samples, modified PTEN residues were identified by Mascot database search of LC-MS/MS data and confirmed by de novo sequencing. The amino acid numbers are indicated on the left and the oxidation sites are in bold red. The oxPTMs

23

detected are indicated by the symbol on top of each modified amino acid, and the position of each modification detected is indicated below each modified residue.

Figure 4. Representative example of peak-picking data review and *de novo* sequencing validating quantification and identification of HOCl-modified peptides. (A) The representative 3D montage zoomed into the feature corresponding to the chlorinated peptide AQEALDFYGEVR, matched across the HOCl-oxidized PTEN samples. The peak picking area drawn by the software algorithm around the peaks (red line) corresponds to the peptide matched across the LC-MS runs aligned for quantification. (B) MS/MS spectrum of the doubly-charged ion at m/z 716.33 identified as AQEALDFY(Cl)GEVR. The tryptic peptide carried a chlorination on Tyr, corresponding to Tyr155 in PTEN. The y1 ion observed at m/z 175 was established as the C-terminal residue R, and used to determine the remaining amino acid residues by calculating the mass difference of adjacent y-ions (labeled using red arrows on the x-axis). By following the y-ion series residues Gln2-Arg12 were sequenced, while Ala1 could not be determined from the above MS/MS spectrum. The chlorinated tyrosine (Y(Cl)) corresponded to a mass shift of 197 Da (163 Da for tyrosine + 34 Da due to the addition of one chlorine).

Figure 5. Relative quantitation of PTEN oxPTMs upon HOCl treatment. Quantification of 20 different modifications detected in either the monomeric protein band at 70 kDa (light grey bars) or the high molecular weight aggregates isolated from the top of the gel (black bars), or both. Vertical axes are % modification and horizontal axes are the ratio of the oxidant to protein (Untr = no oxidant), and data are presented as mean ± SD (n = 3). Cysteine sulfinic acid (e) was only observed in the 70 kDa band whereas Tyr240 oxidation (l), His272 oxidation (o), Trp274 oxidation (p), Tyr377 chlorination (r) and dichlorination (s) and Tyr379 chlorination (t) were only observed in aggregates. For comparison of the effect of oxidant treatments against the untreated control in either monomeric or aggregate protein one-way ANOVA with Dunnett's multiple comparison test was performed (*=p< 0.05, **=p<0.01, ***=p< 0.001, ****=p< 0.0001). For comparison of differences between the 70 kDa band and the high molecular weight aggregates, two-way ANOVA Sidak's multiple comparison test was performed; these differences are discussed in the text.

24

Figure 6. Quantitative mapping of PTEN oxPTMs upon HOCl treatment. (A) The 3D structure map was generated using UCSF Chimera Molecular Modeling System software, highlighting oxidation sites corresponding to a significant increase in modification level for oxPTMs. Residues that were found to be significantly more modified upon HOCl treatment in both intact PTEN-GST and aggregates are highlighted in red. Met134, which was found to be significantly more oxidized only in the PTEN-GST intact band, is highlighted in cyan; Met205, His272, and Trp274, which only showed a significant increase modification levels in the aggregates fractions are highlighted in green. Tyr 377 was also significantly more oxidized in the PTEN aggregates upon HOCl treatment, but is not visible in the 3D model as this region is disordered. (B) The maximum fold change relative to the untreated control and the maximum percentage modification abundance were compared for each oxPTM detected in aggregates or monomeric PTEN bands. Triangles correspond to oxPTMs detected in the 70 kDa band; squares correspond to oxPTMs detected in aggregates. Different colours in the scatterplot correspond to different residues and modifications. Data is presented as the mean of the % maximum relative abundance versus maximum average fold change from three independent experiments for each detected modification.

Table 1. Surface accessibility of selected HOCl-modified residues

Amino acid	Amino acid position	Total	Apolar	Backbone	Sidechain	Ratio (%)	Class assignment [a]
M	35	0	0	0	0	0	Buried
C	71	5.06	0	3.39	1.66	1.6	Buried
M [c]	*134*	*0*	*0*	*0*	*0*	*0*	*Buried*
C	136	0	0	0	0	0	Buried
Y	155	0	0	0	0	0	Buried
M	198	0	0	0	0	0	Buried
M	199	18.13	18.13	0	18.13	11.5	Buried
P	204	0.12	0.12	0.12	0	0	Buried
M [d]	**205**	63.81	58.97	5.15	58.66	37.1	**Intermediate**
M	239	4.7	4.7	0	4.7	3	Buried
Y	240	22.78	8.63	0	22.78	11.8	Buried
C	250	42.32	18.24	7.29	35.03	34.2	Intermediate
M	270	0.62	0	0.62	0	0	Buried
H	**272**	31.53	18.71	0	31.53	20.4	**Intermediate**
W	**274**	25.58	24.98	0	25.58	11.4	Buried
Y	315	59.77	21.64	15.01	44.76	23.2	**Intermediate**

Amino acid	Amino acid position	Relative Surface Accessibility	Absolute Solvent Accessibility	Z-Score	Class assignment [b]
Y	**377**	**0.325**	**69.41**	**-1.253**	**Exposed**
Y	**379**	**0.419**	**89.626**	**-1.669**	**Exposed**

[a] Class assignment was predicted using GETAREA [44] with a probe diameter of 1.4A (equivalent to water) and the 1d5r.pdb 3D-data file from the PDB database. The higher the ratio the more solvent accessible the residue. Ratios <20 are considered buried and >50 exposed. Intermediate values show some solvent accessibility. The C-terminal tail (residue 352 onwards) is disordered in the crystal structure so for this region NetsurfP (ver. 1.1) (http://www.cbs.dtu.dk/services/NetSurfP) was used to predict solvent accessibility of PTEN residues using the PTEN FASTA sequence obtained from Uniprot [45].

[b] Class assignment was predicted using a threshold of 50 exposed accessible surface area, based on the Absolute Solvent Accessibility$_{max}$ of a given amino acid.

[c] Met134, which was found to be significantly more modified exclusively in the PTEN-GST intact band, is indicated in *italics*.

[d] Residues that were found to be significantly more modified exclusively in the aggregates fraction are indicated in **bold.**
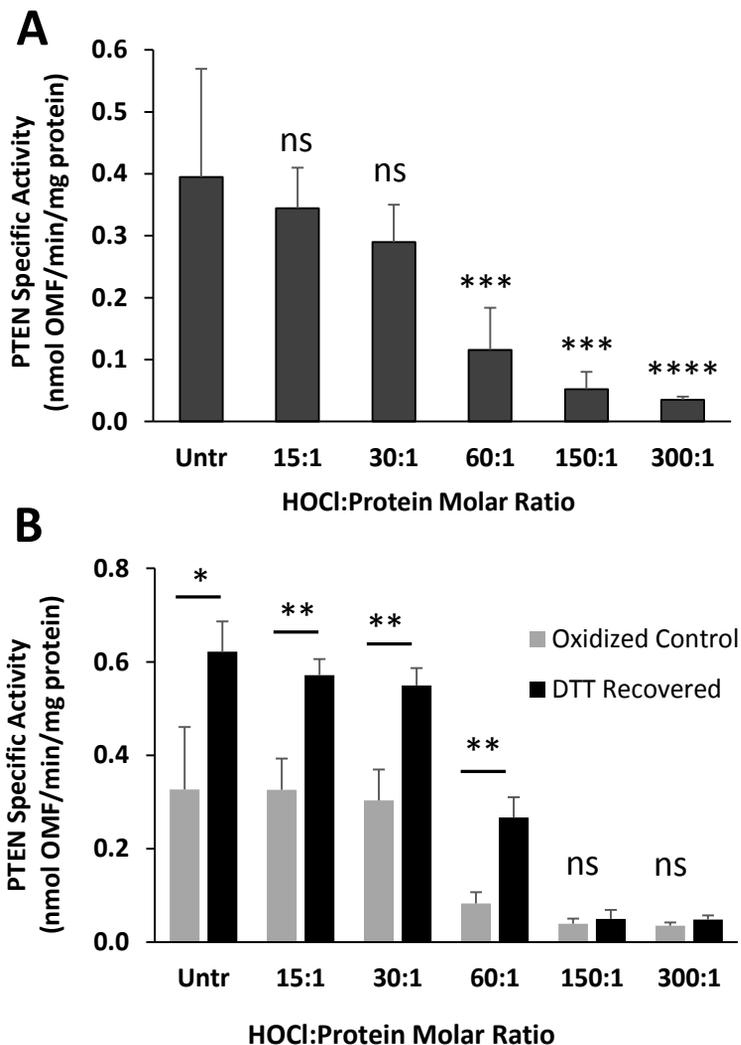
Figure 1. HOCl irreversibly inactivates PTEN. (A) The OMFP assay was used to monitor the effect of increasing HOCl to PTEN-GST molar ratios on PTEN specific activity. The results are presented as mean ± SD (n = 4). Statistical significance for different to the untreated control was assessed by one-way ANOVA followed by Dunnett's correction for multiple comparisons. PTEN specific activity is expressed in nmol OMF/min/mg protein. (B) The effect of DTT reduction on the phosphatase activity of HOCl-oxidized PTEN was evaluated by comparing the specific activity retained by the HOCl-oxidized PTEN before and after recovery with 100 mM DTT. The results are presented as mean ± SD (n = 3). Statistical significance was assessed by two-tailed unpaired Student's t-test for each HOCl:protein ratio. Untr = untreated; * = $p < 0.05$; ** = $p < 0.01$; *** = $p < 0.001$; **** = $p < 0.0001$; ns = not significant).

Figure 2. SDS-PAGE/densitometry analysis versus phosphatase activity of HOCl-oxidized PTEN-GST. (A) Representative (of n=3) coomassie-stained gel of HOCl-oxidized PTEN-GST. 50 μg of protein was loaded per well. Untr = 0 mM HOCl; MW = molecular weight markers. (B) The percentage signal intensity of the Coomassie-stained intact PTEN-GST band and the full gel lane analyzed by densitometry were plotted versus the percentage phosphatase activity as a % of control. Statistical analysis was performed with one-way ANOVA followed by Dunnett's multiple comparisons test before baseline correction. Densitometry data are presented as mean ± SD for N= 3 and activity data are presented as mean ± SD for N = 4 (* = $p < 0.05$; *** = $p < .001$; **** = $p < 0.0001$). (C) Correlation between PTEN phosphatase activity and the protein signal on the gel corresponding to the PTEN-GST band or the full lane. The correlation coefficient r and the p-value were calculated using Pearson's correlation analysis.

Figure 3 PTEN sequence coverage and oxidation sites identified from LC-MS/MS data. For both intact band and aggregate samples, modified PTEN residues were identified by Mascot database search of LC-MS/MS data and confirmed by de novo sequencing. The amino acid numbers are indicated on the left and the oxidation sites are in bold red. The oxPTMs detected are indicated by the symbol on top of each modified amino acid, and the position of each modification detected is indicated below each modified residue.

Figure 4. Representative example of peak-picking data review and *de novo* sequencing validating quantification and identification of HOCl-modified peptides. (A) The representative 3D montage zoomed into the feature corresponding to the chlorinated peptide AQEALDFYGEVR, matched across the HOCl-oxidized PTEN samples. The peak picking area drawn by the software algorithm around the peaks (red line) corresponds to the peptide matched across the LC-MS runs aligned for quantification. (B) MS/MS spectrum of the doubly-charged ion at m/z 716.33 identified as AQEALDFY(Cl)GEVR. The tryptic peptide carried a chlorination on Tyr, corresponding to Tyr155 in PTEN. The y1 ion observed at m/z 175 was established as the C-terminal residue R, and used to determine the remaining amino acid residues by calculating the mass difference of adjacent y-ions (labeled using red arrows on the x-axis). By following the y-ion series residues Gln2-Arg12 were sequenced, while Ala1 could not be determined from the above MS/MS spectrum. The chlorinated tyrosine (Y(Cl)) corresponded to a mass shift of 197 Da (163 Da for tyrosine + 34 Da due to the addition of one chlorine).

Figure 5. Relative quantitation of PTEN oxPTMs upon HOCl treatment. Quantification of 20 different modifications detected in either the monomeric protein band at 70 kDa (light grey bars) or the high molecular weight aggregates isolated from the top of the gel (black bars), or both. Vertical axes are % modification and horizontal axes are the ratio of the oxidant to protein (Untr = no oxidant), and data are presented as mean ± SD (n = 3). Cysteine sulfinic acid (e) was only observed in the 70 kDa band whereas Tyr240 oxidation (l), His272 oxidation (o), Trp274 oxidation (p), Tyr377 chlorination (r) and dichlorination (s) and Tyr379 chlorination (t) were only observed in aggregates. For comparison of the effect of oxidant treatments against the untreated control in either monomeric or aggregate protein one-way ANOVA with Dunnett's multiple comparison test was performed (*=p< 0.05, **=p<0.01, ***=p< 0.001, ****=p< 0.0001). For comparison of differences between the 70 kDa band and the high molecular weight aggregates, two-way ANOVA Sidak's multiple comparison test was performed; these differences are discussed in the text.

Figure 6. Quantitative mapping of PTEN oxPTMs upon HOCl treatment. (A) The 3D structure map was generated using UCSF Chimera Molecular Modeling System software, highlighting oxidation sites corresponding to a significant increase in modification level for oxPTMs. Residues that were found to be significantly more modified upon HOCl treatment in both intact PTEN-GST and aggregates are highlighted in red. Met134, which was found to be significantly more oxidized only in the PTEN-GST intact band, is highlighted in cyan; Met205, His272, and Trp274, which only showed a significant increase modification levels in the aggregates fractions are highlighted in green. Tyr 377 was also significantly more oxidized in the PTEN aggregates upon HOCl treatment, but is not visible in the 3D model as this region is disordered. (B) The maximum fold change relative to the untreated control and the maximum percentage modification abundance were compared for each oxPTM detected in aggregates or monomeric PTEN bands. Triangles correspond to oxPTMs detected in the 70 kDa band; squares correspond to oxPTMs detected in aggregates. Different colours in the scatterplot correspond to different residues and modifications. Data is presented as the mean of the % maximum relative abundance versus maximum average fold change from three independent experiments for each detected modification.

Supplementary Table 1. Identification and quantification of PTEN oxidative modifications in the PTEN-GST intact band and aggregates following HOCl oxidizing treatment.

Peptide sequence[a]	Enzyme[b]	Mod[c]	Fraction detected[d]		HOCl:PTEN-GST molar ratios				
					15:1	30:1	60:1	150:1	300:1
TVEEPSNPEASSSTSVTPDVSDNEPDHYR	Trypsin	Tyr377 CHLOR*	Aggregates	FC	0	Infinity	Infinity	Infinity	Infinity
				p-value	>0.9999	>0.9999	0.6843	0.9908	0.0417
				%	0.00	0.00	0.00	0.01	0.29
FMYFEFPQPLPVCGDIK	Trypsin	Tyr240 OX*	Aggregates	FC	10.06	47.11	84.95	323.25	1031.21
				p-value	0.9997	0.3521	0.0196	0.0001	< 0.0001
				%	0.07	0.60	1.20	2.27	7.24
IYNLCAERHYDTAK	LysC	Cys71 TRIOX*	PTEN-GST band	FC	4.16	8.04	70.11	310.14	405.21
				p-value	> 0.9999	0.9998	0.5733	0.0003	<0.0001
				%	0.12	0.24	2.08	9.20	12.02
FMYFEFPQPLPVCGDIKVEFFHK	LysC	Tyr240 OX*	PTEN-GST band	FC	4.20	5.67	28.18	197.52	226.35
				p-value	> 0.9999	0.9999	0.9868	0.0252	0.0107
				%	0.20	0.27	1.33	9.34	10.70
ADNDKEYLVLTLTK	Trypsin	Tyr315 CHLOR*	PTEN-GST band	FC	1.22	4.82	25.45	88.76	156.24
				p-value	> 0.9999	0.9568	0.0087	< 0.0001	< 0.0001
				%	0.07	0.27	1.44	5.03	8.85
			Aggregates	FC	0.92	0.86	0.80	3.66	3.56
				p-value	0.9999	0.9985	0.9801	0.0131	0.0164
				%	1.39	1.21	2.06	5.52	5.38
GRTGVMICAYLLHRGK	LysC	Cys136 TRIOX*	PTEN-GST band	FC	0.91	1.22	11.59	132.57	131.08
				p-value	> 0.9999	> 0.9999	0.9958	0.0039	0.0042
				%	0.12	0.17	1.58	18.10	17.90
			Aggregates	FC	0.84	0.90	1.48	2.08	2.47
				p-value	0.9381	0.9874	0.2071	0.0023	0.0002
				%	23.61	25.04	41.39	58.32	69.00
TVEEPSNPEASSSTSVTPDVSDNEPDHYR	Trypsin	Tyr377 DICHL*	Aggregates	FC	6.31	9.78	15.99	41.92	71.31
				p-value	0.9916	0.6690	0.4131	0.0305	0.0006
				%	0.92	2.32	3.10	6.09	10.35
FMYFEFPQPLPVCGDIK	Trypsin	Cys250 TRIOX*	PTEN-GST band	FC	1.20	5.64	33.08	51.84	38.82
				p-value	> 0.9999	0.9899	0.0449	0.0022	0.0176
				%	1.60	7.52	44.11	69.12	51.76
			Aggregates	FC	1.77	2.26	3.66	13.20	16.48
				p-value	0.9674	0.2470	0.0020	< 0.0001	< 0.0001
				%	5.34	11.02	22.54	39.74	49.61
YQEDGFDLDLTYIYPNIIAMGFPAER	Trypsin	Met35 DIOX*	PTEN-GST band	FC	1.05	1.07	1.98	14.78	20.67
				p-value	> 0.9999	> 0.9999	0.9982	0.0059	0.0003
				%	0.36	0.37	0.69	5.12	7.16
			Aggregates	FC	5.11	7.48	8.31	23.39	42.33
				p-value	0.7291	0.2585	0.1209	0.0003	< 0.0001
				%	1.13	1.84	2.24	5.18	9.37
MFHFWVNTFFIPGPEETSEK	LysC	Met270 OX*	PTEN-GST band	FC	0.27	0.61	1.92	41.78	27.76
				p-value	0.9999	> 0.9999	0.9999	0.0021	0.0355
				%	0.10	0.24	0.75	16.40	10.89
AQEALDFYGEVRTRDK	LysC	Tyr155 CHLOR*	PTEN-GST band	FC	0.81	1.28	1.71	20.14	24.67
				p-value	> 0.9999	> 0.9999	0.9998	0.0056	0.0011
				%	0.02	0.02	0.03	0.39	0.47
			Aggregates	FC	0.64	0.84	1.65	3.21	2.28
				p-value	0.9864	0.9997	0.864	0.0546	0.3753
				%	0.59	0.76	1.50	2.92	2.08

Peptide	Protease	Modification	Fraction	Measure					
AQEALDF**Y**GEVR	Trypsin	**Tyr155 CHLOR***	PTEN-GST band	FC	0.68	0.84	1.34	8.91	**22.48**
				p-value	0.9997	0.9999	0.9997	**0.0035**	**< 0.0001**
				%	0.32	0.39	0.62	4.14	10.45
			Aggregates	FC	0.91	0.77	0.57	1.52	3.42
				p-value	0.9885	0.2165	0.2214	0.1095	**< 0.0001**
				%	4.70	2.94	2.96	7.91	17.75
TGVMI**C**AYLLHR	Trypsin	**Cys136 DIOX***	PTEN-GST band	FC	2.68	3.71	12.40	**15.39**	3.63
				p-value	0.9952	0.9628	0.1075	**0.0352**	0.9672
				%	0.45	0.62	2.06	2.56	0.60
GRTGV**M**ICAYLLHRGK	Lys C	**Met134 OX***	PTEN-GST band	FC	1.25	1.13	2.58	**14.14**	12.15
				p-value	0.8655	0.8724	0.8247	**0.0178**	**0.0065**
				%	3.44	3.11	7.07	38.81	33.36
TGVMI**C**AYLLHR	Trypsin	**Cys136 TRIOX***	PTEN-GST band	FC	0.87	2.31	5.75	**8.41**	7.85
				p-value	0.9999	0.6478	**0.0040**	**0.0001**	**0.0002**
				%	9.22	24.41	60.64	88.72	82.82
			Aggregates	FC	1.00	1.01	1.04	1.11	1.12
				p-value	> 0.9999	0.5898	0.6901	**0.0064**	**0.0048**
				%	87.18	90.42	90.05	97.07	97.46
MF**H**FWVNTFFIPGPEETSEK	Trypsin	**His272 OX***	Aggregates	FC	1.46	1.68	1.68	4.13	**5.47**
				p-value	0.8268	0.5526	0.6474	**0.0002**	**< 0.0001**
				%	5.50	6.33	6.05	15.58	20.65
TGV**M**ICAYLLHR	Trypsin	**Met134 OX***	PTEN-GST band	FC	0.91	1.64	4.01	**5.05**	4.89
				p-value	0.9998	0.7326	**0.0013**	**0.0001**	**0.0002**
				%	13.07	23.52	57.49	72.39	70.11
			Aggregates	FC	1.03	1.07	1.00	1.10	1.19
				p-value	0.9779	> 0.9999	0.5731	0.2360	**0.0138**
				%	65.55	63.97	68.18	70.35	75.81
MFHFWVNTFFIPGPEETSEK	Trypsin	**Met270 OX***	PTEN-GST band	FC	1.13	1.08	1.47	4.78	**4.86**
				p-value	0.9985	0.9997	0.7986	**< 0.0001**	**< 0.0001**
				%	17.90	17.09	23.27	75.51	76.89
			Aggregates	FC	1.12	1.17	1.23	1.22	1.05
				p-value	0.3084	**0.0172**	**0.0019**	**0.0227**	0.8982
				%	58.51	64.31	68.59	63.78	55.06
MFHF**W**VNTFFIPGPEETSEK	Trypsin	**Trp274 OX***	Aggregates	FC	1.16	1.20	1.04	2.63	**4.86**
				p-value	0.9926	0.9999	0.9997	**0.0065**	**< 0.0001**
				%	8.88	7.98	7.00	20.10	37.18
GRTGVMI**C**AYLLHRGK	LysC	**Cys136 DIOX***	PTEN-GST band	FC	0.00	0.01	0.12	**3.49**	3.35
				p-value	0.9952	0.9628	0.1075	**0.0352**	0.9672
				%	0.00	0.00	0.11	3.14	3.01
MMFETIP**M**FSGGTCNPQFVVCQLK	Trypsin	**Met205 OX***	PTEN-GST band	FC	0.95	0.58	0.57	0.23	2.43
				p-value	> 0.9999	0.9985	0.9985	0.9799	0.8160
				%	0.03	0.02	0.02	0.01	0.09
			Aggregates	FC	2.02	2.64	2.72	**3.41**	3.22
				p-value	0.5278	0.1311	**0.0493**	**0.0254**	**0.0398**
				%	22.71	30.59	35.29	38.40	36.30
F**M**YFEFPQPLPVCGDIK	Trypsin	**Met239 OX***	PTEN-GST band	FC	1.09	1.26	1.80	3.18	**3.34**
				p-value	0.9968	0.8082	**0.0483**	**< 0.0001**	**< 0.0001**
				%	23.06	26.67	38.17	67.24	70.65
			Aggregates	FC	1.21	1.40	1.56	1.97	2.31
				p-value	0.6932	**0.0457**	**0.0354**	**0.0010**	**< 0.0001**
				%	35.0135	44.9442	45.7299	56.9346	66.5483
YQEDGFDLDLTYIYPNIIA**M**GFPAER		Met 35 OX*	PTEN-GST band	FC	1.05	0.99	1.34	1.80	1.74
				p-value	0.9942	0.9999	0.0950	**0.0003**	**0.0006**
				%	52.79	49.61	67.18	90.22	87.34

Peptide[a]	Enzyme[b]	Modification[d]	Gel Fraction[c]						
	Trypsin			FC	0.92	0.99	1.06	1.11	1.24
			Aggregates	p-value	0.9433	0.9819	0.9998	0.8455	0.2735
				%	62.35	72.23	66.89	75.57	84.18
IYNL**C**AER	Trypsin	**Cys71 TRIOX**	PTEN-GST band	FC	1.20	2.62	3.58	4.20	3.42
				p-value	0.9998	0.7290	0.3467	0.1874	0.4026
				%	10.43	22.85	31.23	36.62	29.79
			Aggregates	FC	0.88	0.79	0.74	2.33	2.53
				p-value	0.9998	0.9971	0.9725	0.3804	0.2653
				%	3.72	3.14	2.37	9.84	10.70
TGV**M**ICAYLLHR	Trypsin	Met134 DIOX	PTEN-GST band	FC	0.85	2.59	1.20	0.38	1.01 >
				p-value	0.9997	0.1617	0.9985	0.8523	0.9999
				%	13.07	23.52	57.49	72.39	70.11
GRTGV**M**ICAYLLHRGK	LysC	Met134 DIOX	Aggregates	FC	1.01	0.75	1.02	2.42	2.30
				p-value	> 0.9999	0.9811	> 0.9999	0.0576	0.0866
				%	1.97	1.47	1.99	4.73	4.50
MMFETIPMFSGGTCNPQFVVCQLK	Trypsin	Met198 OX	PTEN-GST band	FC	0.96	1.32	1.27	1.09	1.36
				p-value	0.9999	0.8843	0.9388	0.9997	0.8426
				%	0.35	0.48	0.46	0.40	0.49
			Aggregates	FC	1.53	1.82	1.70	2.00	1.93
				p-value	0.5635	0.3338	0.2112	0.1034	0.1328
				%	38.16	42.23	45.30	49.67	48.18
M**M**FETIPMFSGGTCNPQFVVCQLK	Trypsin	Met199 OX	PTEN-GST band	FC	0.96	1.32	1.26	1.09	1.42
				p-value	0.9999	0.8920	0.9484	0.9989	0.7536
				%	0.35	0.48	0.46	0.40	0.52
			Aggregates	FC	1.57	1.93	1.63	1.86	1.92
				p-value	0.5032	0.6319	0.1596	0.5086	0.4257
				%	30.82	31.98	33.18	36.44	37.67
MMFETI**P**MFSGGTCNPQFVVCQLK	Trypsin	Pro204 OX	PTEN-GST band	FC	1.13	1.39	1.37	0.53	0.70
				p-value	0.9910	0.6105	0.6534	0.4490	0.7928
				%	33.36	41.09	40.49	15.50	20.54
			Aggregates	FC	0.94	0.87	0.97	0.88	0.97
				p-value	0.9965	0.9998	0.9631	0.9543	0.9997
				%	29.24	30.40	34.63	27.57	30.16
MMFETIP**M**FSGGTCNPQFVVCQLK	Trypsin	Met205 DIOX	PTEN-GST band	FC	1.10	0.63	0.37	0.39	0.85
				p-value	0.9998	0.9644	0.7835	0.8006	0.9996
				%	0.09	0.05	0.03	0.03	0.07
VKI**Y**SSNSGPTR	Trypsin	Tyr225 CHLOR	Aggregates	FC	0.99	0.96	1.14	1.35	1.40
				p-value	> 0.9999	0.8106	0.5871	0.1363	0.0780
				%	67.54	77.73	81.32	91.78	95.16
MFHFWVNTFFI**P**GPEETSEK	Trypsin	Pro281 OX	PTEN-GST band	FC	0.37	0.77	0.65	0.00	0.00
				p-value	0.8137	0.9960	0.9770	0.4673	0.4673
				%	0.12	0.25	0.21	0.00	0.00
YSDTTDSDPENEPFDEDQHTQITK	Trypsin	**Tyr379 CHLOR**	Aggregates	FC	7.37	12.40	14.83	170.06	459.86
				p-value	> 0.9999	0.9999	0.9107	0.8143	0.0944
				%	0.26	0.53	4.80	6.03	16.31
GRTGV**M**ICAYLLHRGK	LysC	**Met134 DIOX**	Aggregates	FC	1.01	0.75	1.02	2.42	2.30
				p-value	> 0.9999	0.9811	> 0.9999	0.0576	0.0866
				%	1.97	1.47	1.99	4.73	4.50

a Peptide sequence obtained from the Mascot database search of LC-MS runs aligned on Progenesis QI, carrying the modified residue (in red).

b Enzyme used for the digestion of

c Gel Fraction corresponding to the LC-MS run where the peptide was detected

d Modification type and position within the protein amino acid sequence

F.C = fold change relative to untreated control; p-value was returned by one-way ANOVA with Dunnett's multiple comparison test for each modification detected following relative quantification. % = average percentage abundance of the modification;

Bold indicates more than 2.5-maximum fold change in abundance of the modification in at least one HOCl to PTEN-GST molar ratio used; * indicates modification with a statistically significant increase in abundance, and the significant p-values are highlighted in **bold red**. Infinity indicates FC values obtained when the abundance of the modification in the untreated control was 0.

The data was obtained from the analysis of PTEN-GST intact band and protein aggregates features present in three independent HOCl oxidation experiments.

Ranking of modifications with * is based on maximum FC, highlighted in **bold blue**. Ranking of other modification is based on their position within PTEN structure.

Supplementary Table 2. Surface accessibility of PTEN residues

AA[a]	AA position[b]	RSA[c]	ASA[d]	Z-Score	Class assignment
M	1	0.625	125.143	-2.026	Exposed
T	2	0.425	58.892	-0.289	Exposed
A	3	0.495	54.582	-0.833	Exposed
I	4	0.307	56.832	0.949	Exposed
I	5	0.162	30.062	-0.631	Buried
K	6	0.274	56.465	0.904	Buried
E	7	0.421	73.619	0.447	Exposed
I	8	0.103	19.073	0.663	Buried
V	9	0.098	15.124	-0.324	Buried
S	10	0.416	48.708	-0.458	Exposed
R	11	0.494	113.24	0.467	Exposed
N	12	0.345	50.523	0.018	Exposed
K	13	0.441	90.631	-0.405	Exposed

AA[a]	AA position[b]	Total	Apolar	Backbone	Sidechain	Ratio (%)	Class assignment
R	14	223.13	109.05	27.57	195.57	100	e
R	15	105.18	39.11	7.18	98	50.1	e
Y	16	102.3	64.06	4.34	97.96	50.7	e
Q	17	71.89	8.43	17.93	53.96	37.6	i
E	18	31.36	10.42	9.65	21.71	15.4	b
D	19	100.54	37.05	30.35	70.19	62.1	e
G	20	68.42	35.77	68.42	0	78.5	e
F	21	83.85	69.03	29.11	54.74	30.4	i
D	22	96.71	29.6	14.88	81.83	72.4	e
L	23	13.41	13.41	1.75	11.66	8	b
D	24	32.49	11.81	0.24	32.25	28.5	i
L	25	0.49	0.1	0.39	0.1	0.1	b
T	26	3.44	3.44	2.02	1.42	1.3	b
Y	27	39.59	38.2	1.08	38.51	19.9	b
I	28	6.52	0	6.52	0	0	b
Y	29	36.99	36.21	5.36	31.63	16.4	b
P	30	114.09	109.51	11.45	102.64	97.6	e
N	31	41.62	9.54	0.25	41.38	36.2	i
I	32	5.99	5.99	0	5.99	4.1	b
I	33	0	0	0	0	0	b
A	34	0	0	0	0	0	b
M	35	0	0	0	0	0	b
G	36	2.05	2.05	2.05	0	2.4	b
F	37	7.1	5.07	2.05	5.05	2.8	b
P	38	0	0	0	0	0	b
A	39	1.04	0.74	0.36	0.69	1.1	b
E	40	93.03	29	26.3	66.72	47.3	i

R	41	190.84	87.36	10.07	180.77	92.5	e
L	42	79.45	75.1	4.35	75.1	51.4	e
E	43	123.71	46.35	13.95	109.77	77.7	e
G	44	66.83	47.58	66.83	0	76.6	e
V	45	91.43	83.93	14.75	76.68	62.7	e
Y	46	29.42	24.85	5.07	24.36	12.6	b
R	47	180.11	74.06	15.84	164.27	84	e
N	48	5.78	3.21	3.16	2.63	2.3	b
N	49	59.73	5.01	0.63	59.1	51.7	e
I	50	4.56	4.56	0	4.56	3.1	b
D	51	64.65	14.92	1.62	63.03	55.8	e
D	52	45.27	3.52	0	45.27	40.1	i
V	53	0	0	0	0	0	b
V	54	23.14	23.14	0	23.14	18.9	b
R	55	131.63	69.96	6.77	124.86	63.9	e
F	56	0	0	0	0	0	b
L	57	0	0	0	0	0	b
D	58	45.25	27.53	5.98	39.27	34.8	i
S	59	80.59	52.74	41.11	39.48	51	e
K	60	97.55	63.22	29.79	67.76	41.2	i
H	61	24.44	18.04	6.48	17.97	11.6	b
K	62	149.21	108.18	5.16	144.04	87.6	e
N	63	92.69	35.83	9.85	82.83	72.5	e
H	64	61.27	42.64	0.07	61.2	39.6	i
Y	65	1.72	0.14	1.58	0.14	0.1	b
K	66	22.24	2.34	0	22.24	13.5	b
I	67	0	0	0	0	0	b
Y	68	0	0	0	0	0	b
N	69	0.49	0	0.02	0.46	0.4	b
L	70	0	0	0	0	0	b
C	71	5.06	0	3.39	1.66	1.6	b
A	72	40.75	16.66	26.28	14.47	22.3	i
E	73	80.91	45.69	30.71	50.2	35.6	i
R	74	130.96	56.78	6.42	124.54	63.7	e
H	75	76.3	55.17	19.37	56.93	36.8	i
Y	76	6.69	5.9	6.69	0	0	b
D	77	113.28	34.01	9.09	104.2	92.2	e
T	78	48.42	9.98	8.76	39.66	37.3	i
A	79	84.99	66.63	34.64	50.35	77.6	e
K	80	101.7	78.35	14.97	86.73	52.7	e
F	81	4.85	0	4.85	0	0	b
N	82	90.64	30.88	15.63	75.01	65.6	e
C	83	39.95	22.13	36.7	3.24	3.2	b
R	84	149.84	75.13	7.8	142.04	72.7	e
V	85	8.02	3.41	4.62	3.4	2.8	b
A	86	9.48	9.48	1.63	7.85	12.1	b
Q	87	94.74	16.57	21.95	72.79	50.7	e
Y	88	30.29	18.54	0.61	29.67	15.4	b
P	89	67.22	54.69	12.53	54.69	52	e

F	90	14.04	14.04	5.68	8.35	4.6	b
E	91	74.36	34.38	0.29	74.06	52.5	e
D	92	54.59	24.33	8.96	45.63	40.4	i
H	93	114.36	90	3.99	110.37	71.4	e
N	94	23.66	2.24	0.71	22.95	20.1	i
P	95	8.23	1.27	6.97	1.27	1.2	b
P	96	1.63	0.99	1.63	0	0	b
Q	97	97.29	22.52	2.2	95.09	66.2	e
L	98	4.54	3.5	1.04	3.5	2.4	b
E	99	105.29	34.87	8.27	97.02	68.7	e
L	100	41.59	41.57	3.01	38.58	26.4	i
I	101	0.31	0.31	0	0.31	0.2	b
K	102	96.77	73.04	0.03	96.73	58.8	e
P	103	62.95	60.57	4.2	58.75	55.8	e
F	104	0	0	0	0	0	b
C	105	0	0	0	0	0	b
E	106	76.23	30.42	4.36	71.87	50.9	e
D	107	32.68	16.81	10.04	22.64	20	i
L	108	0	0	0	0	0	b
D	109	41.6	0.35	0.13	41.47	36.7	i
Q	110	93.42	34.86	2.28	91.14	63.4	e
W	111	24.48	24.48	0	24.48	10.9	b
L	112	18.33	7.22	11.12	7.22	4.9	b
S	113	70.47	51.28	29.25	41.22	53.3	e
E	114	108.9	61.82	22.8	86.1	61	e
D	115	62.26	25.98	38.04	24.22	21.4	i
D	116	93.7	18.6	33.31	60.39	53.4	e
N	117	25.01	2.72	2.72	22.29	19.5	b
H	118	68.86	55.41	0	68.86	44.5	i
V	119	6.42	6.42	0	6.42	5.2	b
A	120	0	0	0	0	0	b
A	121	0.01	0.01	0	0.01	0	b
I	122	0	0	0	0	0	b
H	123	0	0	0	0	0	b
C	124	4.86	0	0	4.86	4.8	b
K	125	39.52	17.97	2.61	36.9	22.4	i
A	126	46.97	40.96	8.24	38.73	59.7	e
G	127	1.19	0	1.19	0	1.4	b
K	128	87.8	83.55	0.27	87.53	53.2	e
G	129	10.09	8.85	10.09	0	11.6	b
R	130	7.19	3.11	0.56	6.63	3.4	b
T	131	0	0	0	0	0	b
G	132	0	0	0	0	0	b
V	133	0	0	0	0	0	b
M	134	0	0	0	0	0	b
I	135	0	0	0	0	0	b
C	136	0	0	0	0	0	b
A	137	0	0	0	0	0	b
Y	138	6.39	2.45	0	6.39	3.3	b

L	139	1.95	1.95	0	1.95	1.3	b
L	140	10.76	1.63	9.16	1.6	1.1	b
H	141	48.45	23.73	18.54	29.9	19.3	b
R	142	146.16	39.7	19	127.16	65	e
G	143	42.16	22.98	42.16	0	48.3	i
K	144	117.6	65.86	19.52	98.08	59.6	e
F	145	37.9	37.78	1.95	35.95	20	b
L	146	136.85	129.59	9.16	127.68	87.3	e
K	147	126.69	90.14	2.03	124.66	75.8	e
A	148	3	2.12	0.88	2.12	3.3	b
Q	149	100.77	22.34	0.15	100.62	70	e
E	150	67.68	36.32	9.44	58.24	41.2	i
A	151	0	0	0	0	0	b
L	152	4.47	0.39	4.08	0.39	0.3	b
D	153	70.53	26.32	7.95	62.58	55.4	e
F	154	57.22	57.22	3.13	54.08	30	i
Y	155	0	0	0	0	0	b
G	156	2.47	2.47	2.47	0	2.8	b
E	157	77.34	15.54	0.89	76.45	54.1	e
V	158	28.45	28.45	0.98	27.46	22.5	i
R	159	10.17	5.49	0.26	9.91	5.1	b
T	160	12.67	12.42	0.25	12.42	11.7	b
R	161	139.76	62.73	28.98	110.77	56.7	e
D	162	73.48	38.8	15.77	57.71	51.1	e
K	163	145.82	88.33	21	124.82	75.9	e
K	164	113.69	74.64	0.85	112.83	68.6	e
G	165	3.34	1.07	3.34	0	3.8	b
V	166	3.44	0.18	3.26	0.18	0.1	b
T	167	37.46	25.66	8.36	29.1	27.4	i
I	168	30.2	30.2	0.32	29.88	20.3	i
P	169	11.56	10.55	1.63	9.93	9.4	b
S	170	0.09	0.09	0	0.09	0.1	b
Q	171	0.57	0	0	0.57	0.4	b
R	172	60.97	32.48	0	60.97	31.2	i
R	173	30.38	21.53	6.45	23.93	12.2	b
Y	174	0.07	0.07	0	0.07	0	b
V	175	0	0	0	0	0	b
Y	176	94.9	84.79	2.61	92.29	47.8	i
Y	177	20.92	18.76	0.51	20.41	10.6	b
Y	178	3.86	2.91	0	3.86	2	b
S	179	5.63	3.11	1.16	4.48	5.8	b
Y	180	98.71	64.47	1.15	97.56	50.5	e
L	181	9.01	8.7	0.31	8.7	6	b
L	182	54.31	51.04	6.95	47.36	32.4	i
K	183	125.09	95.21	27.32	97.77	59.4	e
N	184	60.66	13.56	21.21	39.45	34.5	i
H	185	161.65	119.85	29.09	132.57	85.7	e

L	186	77.61	68.27	13.53	64.08	43.8	i
D	187	108.01	34.38	10.3	97.71	86.5	e
Y	188	34.36	15.26	16.25	18.1	9.4	b
R	189	170.47	75.89	1.14	169.33	86.6	e
P	190	95.65	78.22	17.43	78.22	74.4	e
V	191	42.89	42.89	3.7	39.19	32	i
A	192	47.41	42.12	5.29	42.12	64.9	e
L	193	0.31	0.04	0.27	0.04	0	b
L	194	53.88	53.88	0	53.88	36.9	i
F	195	0.14	0.14	0	0.14	0.1	b
H	196	43.72	28.36	5.24	38.48	24.9	i
K	197	31.65	8.29	0	31.65	19.2	b
M	198	0	0	0	0	0	b
M	199	18.13	18.13	0	18.13	11.5	b
F	200	0	0	0	0	0	b
E	201	41.55	7.94	1.09	40.46	28.7	i
T	202	31.35	30.8	0.01	31.34	29.5	i
I	203	21.94	15.83	6.28	15.66	10.6	b
P	204	0.12	0.12	0.12	0	0	b
M	205	63.81	58.97	5.15	58.66	37.1	i
F	206	38.11	14.14	28.34	9.77	5.4	b
S	207	42.26	18.31	15.74	26.52	34.3	i
G	208	85.78	57.06	85.78	0	98.4	e
G	209	46.34	33.65	46.34	0	53.1	e
T	210	54.49	34.95	0	54.49	51.3	e
C	211	7.6	0.82	7.6	0	0	b
N	212	65.84	6.51	0.97	64.88	56.8	e
P	213	0.19	0.07	0.12	0.07	0.1	b
Q	214	9.5	1.03	0.37	9.13	6.4	b
F	215	5.56	5.56	0	5.56	3.1	b
V	216	29.15	28.47	0.67	28.47	23.3	i
V	217	0	0	0	0	0	b
C	218	24.08	1.52	0	24.08	23.5	i
Q	219	43.93	3.08	0.27	43.66	30.4	i
L	220	84.89	82.82	4.89	80.01	54.7	e
K	221	176.37	110.59	33.3	143.07	87	e
V	222	98.18	98.18	3.69	94.49	77.3	e
K	223	149.85	91.3	14.21	135.64	82.5	e
I	224	60.44	38.19	30.15	30.3	20.6	i
Y	225	54.73	40.95	7.04	47.68	24.7	i
S	226	72.4	33.67	19.86	52.54	67.9	e
S	227	15.64	8.81	8.83	6.81	8.8	b
N	228	119.12	58.93	17.07	102.06	89.3	e
S	229	52.02	34.19	13.83	38.19	49.3	i
G	230	22.46	16.76	22.46	0	25.8	i
P	231	35.5	17.43	18.09	17.41	16.6	b
T	232	78.82	51.97	39.9	38.92	36.6	i
R	233	105.48	73.5	7.64	97.84	50	e
R	234	114.6	52.15	24.05	90.55	46.3	i

E	235	79.99	45.32	9.1	70.89	50.2	e
D	236	99.17	43.85	9.63	89.54	79.2	e
K	237	127.61	87	0.71	126.89	77.1	e
F	238	59.52	59.52	0	59.52	33	i
M	239	4.7	4.7	0	4.7	3	b
Y	240	22.78	8.63	0	22.78	11.8	b
F	241	2.78	2.68	0.41	2.37	1.3	b
E	242	66.83	18.59	8.05	58.78	41.6	i
F	243	12.82	1.18	11.81	1.01	0.6	b
P	244	98.74	78.59	34.67	64.07	60.9	e
Q	245	128.06	68.32	4.61	123.45	85.9	e
P	246	62.79	55.68	7.42	55.37	52.6	e
L	247	13.06	13.06	2.38	10.69	7.3	b
P	248	95.59	92.37	3.23	92.36	87.8	e
V	249	2.76	1.98	2.76	0	0	b
C	250	42.32	18.24	7.29	35.03	34.2	i
G	251	13.53	13.53	13.53	0	15.5	b
D	252	10.06	1.15	1.5	8.56	7.6	b
I	253	3.43	3.43	0	3.43	2.3	b
K	254	43.04	9.36	0.02	43.03	26.2	i
V	255	0.36	0.36	0	0.36	0.3	b
E	256	27.29	2.09	0	27.29	19.3	b
F	257	0.03	0	0.03	0	0	b
F	258	21.21	21.21	0	21.21	11.8	b
H	259	0.47	0.47	0	0.47	0.3	b
K	260	66.99	47.95	3.55	63.44	38.6	i
Q	261	44.34	14.74	6.61	37.73	26.3	i
N	262	92.57	43.07	15.02	77.55	67.8	e
K	263	195.49	141.34	36.12	159.38	96.9	e
M	264	111.29	99	21.23	90.07	56.9	e
L	265	190.76	171.01	27.66	163.11	100	e
K	266	134.4	94.91	14.2	120.2	73.1	e
K	267	78.71	25.7	14.03	64.69	39.3	i
D	268	60.14	18.07	5.85	54.29	48	i
K	269	97.57	84.55	4	93.57	56.9	e
M	270	0.62	0	0.62	0	0	b
F	271	0.6	0.48	0.6	0	0	b
H	272	31.53	18.71	0	31.53	20.4	i
F	273	0.79	0.79	0	0.79	0.4	b
W	274	25.58	24.98	0	25.58	11.4	b
V	275	2.74	2.74	0	2.74	2.2	b
N	276	0.43	0	0	0.43	0.4	b
T	277	0.19	0.19	0	0.19	0.2	b
F	278	32.44	24.88	7.55	24.88	13.8	b
F	279	29.9	12.19	20.48	9.42	5.2	b
I	280	18.35	1.08	17.35	1	0.7	b
P	281	82.58	54.28	54.76	27.82	26.4	i
G	282	247.54	161.65	67.66	179.88	100	e
P	283	146.54	44.25	40.34	106.19	75.2	e

E	284	59.77	21.64	15.01	44.76	23.2	i
E	285	33.8	33.8	10.43	23.38	16	b
T	286	69.58	41.97	27.62	41.95	34.3	i
S	287	43.54	43.54	1.9	41.64	28.5	i
E	288	59.02	20.1	14.3	44.71	42.1	i
K	289	8.46	8.46	0	8.46	5.8	b
V	290	48.32	44.23	0	48.32	45.5	i
E	291	15.32	14.57	0.02	15.3	9.3	b
N	292	103.91	28.56	9.41	94.5	82.7	e
G	293	49.68	5.6	2.07	47.61	42.1	i
S	294	0	0	0	0	0	b
L	295	10.16	1.69	8.03	2.13	1.9	b
C	296	98.62	75.72	5.24	93.38	56.8	e
D	297	1.25	1.25	1.25	0	0	b
Q	298	13.14	4.49	1.88	11.26	9.9	b
E	299	116.76	67.96	17.26	99.5	60.5	e
I	300	18.34	14.86	9.11	9.23	8.2	b
D	301	146.01	109.15	20.17	125.83	76.5	e
S	302	77.13	65.55	27.15	49.99	77	e
I	303	59.06	13.63	11.78	47.28	41.4	i
C	304	168.36	64.7	13.78	154.58	79.1	e
S	305	107.27	66.86	0	107.27	55.6	e
I	306	2.83	2.83	0.37	2.45	1.4	b
E	307	29.93	28.64	0.47	29.46	38.1	i
R	308	74.31	74.31	4.09	70.22	66.8	e
A	309	103.17	25.6	15.38	87.79	76.8	e

AA[a]	AA position[b]	RSA[c]	ASA[d]	Z-Score	Class assignment[e]
D	310	0.424	61.026	-1.278	Exposed
N	311	0.44	64.401	-2.283	Exposed
D	312	0.369	53.216	-2.157	Exposed
K	313	0.277	56.897	-1.363	Buried
E	314	0.316	55.258	-1.470	Exposed
Y	315	0.177	37.932	0.048	Buried
L	316	0.092	16.809	-0.174	Buried
V	317	0.097	14.863	0.417	Buried
L	318	0.041	7.58	-0.148	Buried
T	319	0.273	37.851	0.733	Exposed
L	320	0.031	5.694	0.612	Buried
T	321	0.403	55.868	0.548	Exposed
K	322	0.227	46.714	0.052	Buried
N	323	0.517	75.689	-0.953	Exposed
D	324	0.391	56.386	-0.797	Exposed
L	325	0.098	17.999	-0.515	Buried
D	326	0.193	27.811	-0.911	Buried
K	327	0.62	127.616	-0.058	Exposed
A	328	0.316	34.867	-1.196	Exposed
N	329	0.274	40.172	-0.312	Buried

K	330	0.555	114.122	-0.170	Exposed
D	331	0.508	73.26	-0.896	Exposed
K	332	0.59	121.363	0.184	Exposed
A	333	0.546	60.202	0.237	Exposed
N	334	0.309	45.238	0.043	Exposed
R	335	0.682	156.178	0.613	Exposed
Y	336	0.332	71.034	0.663	Exposed
F	337	0.061	12.323	0.919	Buried
S	338	0.319	37.363	0.887	Exposed
P	339	0.758	107.503	-0.106	Exposed
N	340	0.63	92.217	0.415	Exposed
F	341	0.043	8.59	-0.172	Buried
K	342	0.427	87.875	1.712	Exposed
V	343	0.052	7.962	0.22	Buried
K	344	0.192	39.556	0.917	Buried
L	345	0.066	12.14	0.321	Buried
Y	346	0.16	34.256	0.832	Buried
F	347	0.043	8.65	-0.603	Buried
T	348	0.333	46.187	0.269	Exposed
K	349	0.555	114.225	0.06	Exposed
T	350	0.209	29.058	0.074	Buried
V	351	0.433	66.475	-0.384	Exposed
E	352	0.563	98.286	-0.035	Exposed
E	353	0.622	108.646	0.17	Exposed
P	354	0.262	37.22	-0.597	Exposed
S	355	0.67	78.524	0.089	Exposed
N	356	0.578	84.605	-0.571	Exposed
P	357	0.491	69.687	-1.625	Exposed
E	358	0.708	123.757	-0.558	Exposed
A	359	0.272	29.93	-0.330	Buried
S	360	0.536	62.772	-0.547	Exposed
S	361	0.62	72.711	-1.781	Exposed
S	362	0.462	54.1	-0.984	Exposed
T	363	0.543	75.342	-0.723	Exposed
S	364	0.615	72.031	-0.832	Exposed
V	365	0.276	42.452	-0.380	Exposed
T	366	0.484	67.089	-0.052	Exposed
P	367	0.405	57.498	-1.305	Exposed
D	368	0.566	81.546	-1.095	Exposed
V	369	0.324	49.799	-0.405	Exposed
S	370	0.37	43.329	-0.989	Exposed
D	371	0.625	90.077	-1.035	Exposed
N	372	0.623	91.163	-1.923	Exposed
E	373	0.534	93.22	-0.386	Exposed
P	374	0.287	40.754	-1.197	Buried
D	375	0.54	77.785	-1.074	Exposed
H	376	0.345	62.701	-0.945	Exposed
Y	377	0.325	69.41	-1.253	Exposed
R	378	0.612	140.217	-0.378	Exposed

AA	Position	RSA	ASA		Class
Y	379	0.419	89.626	-1.669	Exposed
S	380	0.434	50.877	-1.696	Exposed
D	381	0.652	93.939	-1.746	Exposed
T	382	0.386	53.483	-0.547	Exposed
T	383	0.484	67.145	-2.135	Exposed
D	384	0.651	93.751	-1.375	Exposed
S	385	0.577	67.624	-1.643	Exposed
D	386	0.411	59.153	-0.394	Exposed
P	387	0.446	63.231	-0.994	Exposed
E	388	0.595	103.859	-0.758	Exposed
N	389	0.644	94.34	-0.928	Exposed
E	390	0.422	73.776	-0.732	Exposed
P	391	0.604	85.651	-1.141	Exposed
F	392	0.368	73.898	-1.544	Exposed
D	393	0.403	58.043	-0.967	Exposed
E	394	0.475	82.948	-2.052	Exposed
D	395	0.472	68.087	-1.271	Exposed
Q	396	0.289	51.633	-0.103	Buried
H	397	0.241	43.82	0.088	Buried
T	398	0.166	23.094	-0.150	Buried
Q	399	0.452	80.799	0.882	Exposed
I	400	0.129	23.958	-0.236	Buried
T	401	0.479	66.465	0.851	Exposed
K	402	0.562	115.645	0.516	Exposed
V	403	0.68	104.455	-0.634	Exposed

a AA=Amino acid. Residues 1-13 and the C-terminal tail (residue 352 onwards) are disordered in the crystal structure so for this region NetsurfP (ver. 1.1) (http://www.cbs.dtu.dk/services/NetSurfP) was used to predict solvent accessibility of PTEN residues using the PTEN FASTA sequence obtained from Uniprot [36]. Class assignment was predicted using a threshold of 50 exposed accessible surface area, based on the Absolute Solvent Accessibilitymax of a given amino acid. For Residues 14-351, class assignment was predicted using GETAREA with a probe diameter of 1.4A (equivalent to water) and the 1d5r.pdb 3D-data file from the PDB database. The higher the ratio the more solvent accessible the residue. Ratios <20 are considered buried and >50 exposed. Intermediate values show some solvent accessibility.

b Amino acid position

c RSA= Relative Surface Accessibility

d ASA= Absolute Solvent Accessibility
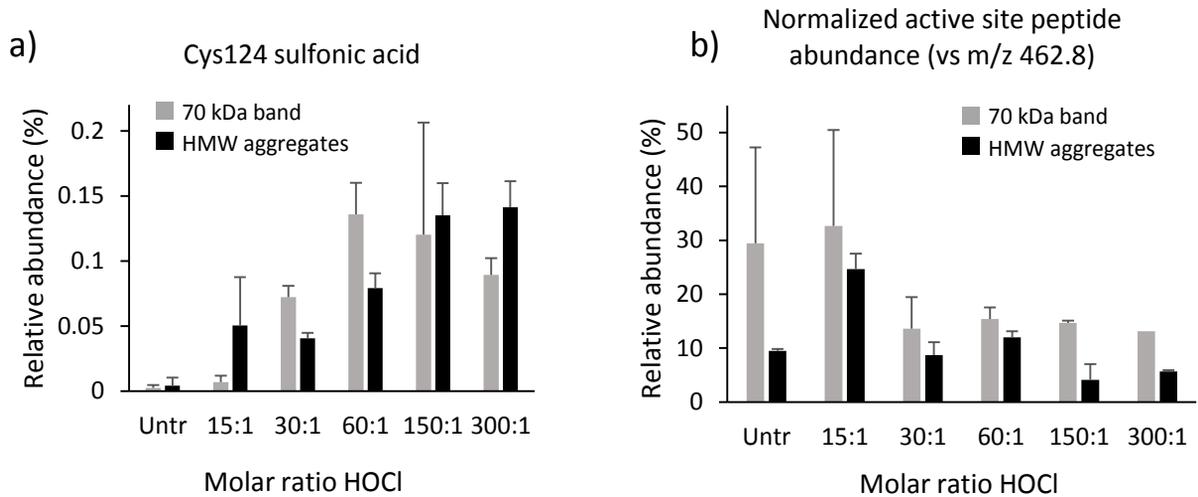
Supplementary figure 1. Active site cysteine modification. Quantification of a) the cysteine sulfonic acid forms of the observed active site (Cys124) containing peptide and b) the intensity of the unmodified active site containing peptide normalized to another PTEN peptide (m/z 462.8, residues 190-197, PVALLFHK). Light grey bars represent the monomeric protein band at 70 kDa and black bars the high molecular weight aggregates isolated from the top of the gel. The vertical axes are % modification, the horizontal axes are the molar ratio of HOCl to protein (Untr = no oxidant), and data are presented as mean ± SD (n = 3).
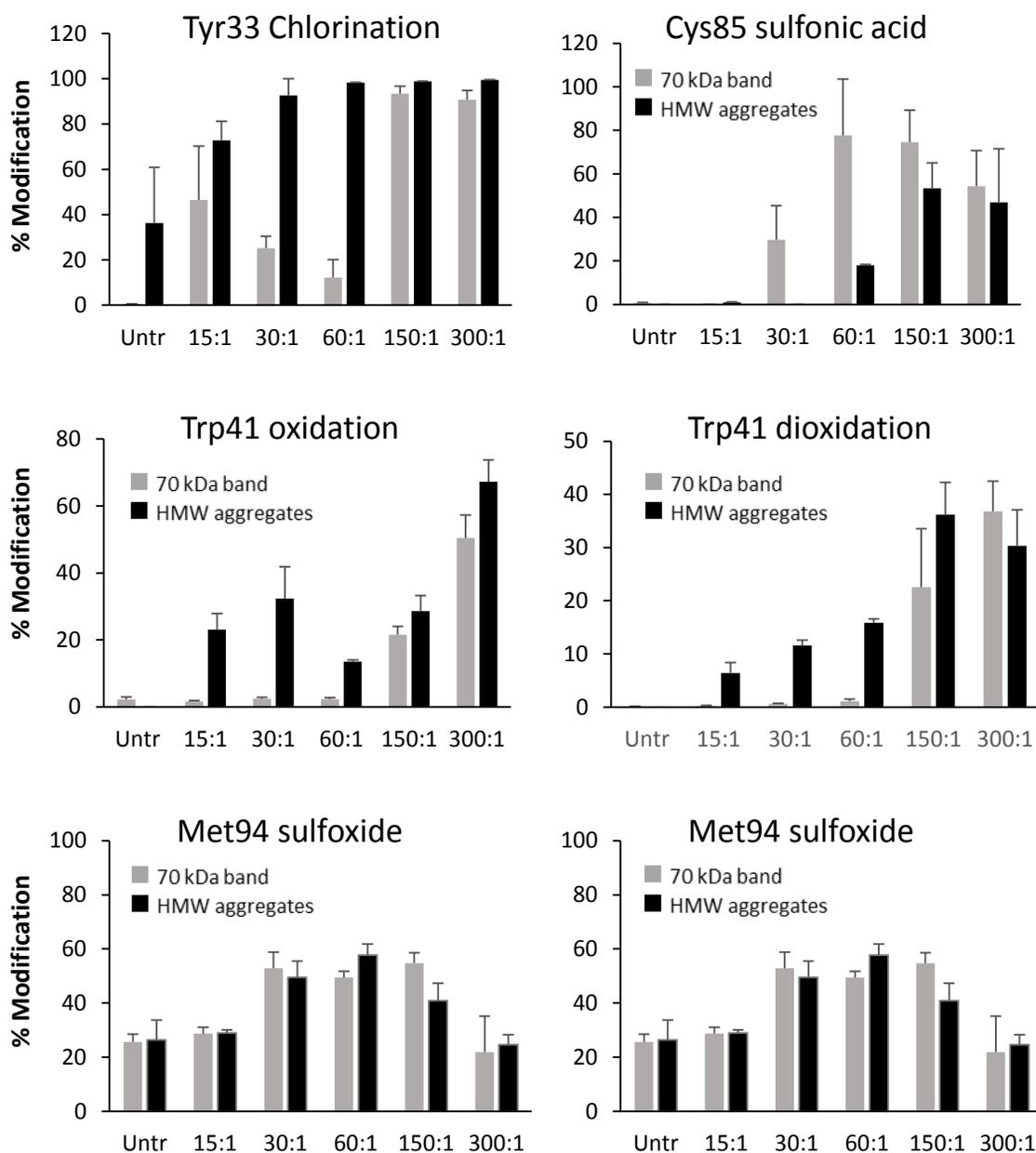
Supplementary figure 2. Relative quantitation of selected GST oxPTMs upon HOCl treatment. Quantification of 6 different modifications detected in either the monomeric protein band at 70 kDa (light grey bars) or the high molecular weight aggregates isolated from the top of the gel (black bars), or both. The vertical axes are the percentage (%) of peptide modified, the horizontal axes are the molar ratio of HOCl to protein (Untr = no oxidant), and data are presented as mean ± SD (n = 3).